SIMULATIONS OF THE FLOW OF A HYDROCARBON FUEL UNDER DIFFERENT BODY FORCE CONDITIONS

Thesis

Submitted to

The School of Engineering

UNIVERSITY OF DAYTON

In Partial Fulfillment of the Requirements for

The Degree

Master of Science in Mechanical Engineering

By

Michael Timothy Frede

UNIVERSITY OF DAYTON

Dayton, Ohio

July 2007

Simulations of the Flow of a Hydrocarbon Fuel under Different Body Force Conditions

APPROVED BY:

Jamie Ervin, Ph.D.
Committee Chair
Professor, Mechanical and Aerospace Engineering Department

Timothy Fry, Ph.D.
Committee Co-chair
Adjunct Assistant Professor, Mechanical and Aerospace Engineering Department

Vinod Jain, Ph.D.
Committee Member
Professor, Mechanical and Aerospace Engineering Department

Malcolm W. Daniels, Ph.D.
Associate Dean
School of Engineering

Joseph E. Saliba, Ph.D. P.E.
Dean, School of Engineering

ABSTRACT

SIMULATIONS OF THE FLOW OF A HYDROCARBON FUEL UNDER DIFFERENT BODY FORCE CONDITIONS

Name: Michael Frede
University of Dayton, 2007

Advisor: Dr. Jamie Ervin and Dr. Timothy Fry

The primary focus of this thesis is on the analysis of jet fuel, specifically JP-10, as it moves through various internal flow paths whose external walls are subject to various heat fluxes. A straight tube, a bent tube, and a rotating disk are all analyzed using the software program Fluent and the material database REFPROP. Primarily, buoyancy forces and centripetal forces are examined. The effects such as vortices of both can be seen on the fuel flow. The three-dimensional models used to analyze the JP-10 are also compared to the two-dimensional models used in Katta's simulations (2005). The three-dimensional models do not require the boundary profile at the velocity inlet that the two-dimensional model does. The three-dimensional model also reveals more about the vortices cause by heating and rotation.

ACKNOWLEDGEMENTS

My special thanks go to Jamie Ervin for his time, his guidance, his personal experience, and his patience in helping to complete my thesis work. I would also like to thank Wright Patterson Air Force Base and the University of Dayton Research Institute for providing the materials, equipment, and facility necessary to do the research in a quality manner. A special thanks to DAGSI for their financial support without which this project would not have been possible.

I want to express my sincere appreciation to Dr. Tim Fry for making me feel like part of his group and for his support whenever I needed it. I cannot thank Mike Swindeman enough for listening to me, being a friend, and doing whatever he could to help me through this thesis.

My acknowledgements would not be complete without thanking my parents for their unconditional love, constant encouragement, and support of my continuing education. Thanks Mom and Dad.

TABLE OF CONTENTS

LIST OF FIGURES

LIST OF TABLES

LIST OF SYMBOLS

C_p	specific heat at constant pressure
C_v	specific heat at constant volume
d	diameter
E	energy
$\vec{F}$	external body forces
$\vec{g}$	gravity
I	identity matrix
k	thermal conductivity
k_{eff}	effective thermal conductivity
n	coefficient of the equation for the real gas Helmholtz energy resulting from intermolecular forces
P	operating pressure
Re	Reynolds number
S_h	potential radiation and volumetric heat sources
S_m	mass source
T	temperature
T_c	critical temperature
t	time
$\vec{v}$	velocity

a	Helmholtz energy
$a^0(\rho,T)$	Ideal gas contribution to the Helmholtz energy
$a^r(\rho,T)$	Real gas Helmholtz energy that results from intermolecular forces
δ	Dimensionless density - ρ/ρ_c
μ	Viscosity
ρ	Density
ρ_c	Critical density
τ	Dimensionless temperature - T_c/T
$\bar{\bar{\tau}}$	Stress Tensor
∇	Gradient – vector derivative of a scalar field

CHAPTER 1

INTRODUCTION

1.1 Background

The four major forces on an aircraft are the weight, drag, lift, and thrust. All of these can be adjusted by the design of the aircraft. In the case of jet aircraft, the goal is to achieve the most thrust, the highest lift to drag ratio, and the least weight. Reducing weight increases the maximum velocity of the aircraft and increases the lift to drag ratio. Thus, weight has a major effect on the flight characteristics of jets. One way to minimize the aircraft weight is to use jet fuel as a coolant in various components and sub-systems. Rather than carrying a separate fluid on board as a coolant, fuel is used to cool aircraft components such as avionics and electrical systems to keep them at a safe operating temperature.

With new generations of aircraft engines, their power has increased. Unfortunately, the waste heat generated by the engine and aircraft systems has also increased. Some current aircraft have resorted to circulating fuel back to a fuel tank via an air/fuel heat exchanger after it has been used in a cooling application. This heat exchanger system limits the maximum fuel temperature in the tank, but the approach adds weight and other penalties (Edwards, USAF Supercritical Hydrocarbon Fuels Interests). Thus, an important focus of fuel development has been the increase of thermal stability at

higher temperatures so that a once through system can be used (i.e. non-recirculating). Hydrocarbon fuels have a tendency to degrade when exposed to higher temperatures. Thermal stability is the ability of the fuel to resist degradation in the presence of heat. A fuel with a high thermal stability will resist degradation less when exposed to relatively high temperatures.

One option may be the use of fuels at supercritical temperatures when the fuel is acting as a coolant. Supercritical temperatures and pressures are above the thermodynamic critical point of a fluid. This is the point at which significant differences between the liquid and gas phases cease to exist. The rapid increase in specific heat, C_v, as the critical temperature is approached is an indication of the supercritical phase. In this phase, the fuel has a liquid-like density and gas-like viscosity and speed of sound. Supercritical fluids have no surface tension and have been used as solvents (Edwards, USAF Supercritical Hydrocarbon Fuels Interests). Thermal stability and fuel injection are two problem areas that need to be addressed when using supercritical fuels. The thermal stability of fuels at subcritical temperatures and pressures is not well understood. Relatively less is known about fuel degradation physical and chemical processes at supercritical conditions. For example, near the critical point the diffusivity of solutes in supercritical fluids becomes very pressure dependent and can be varied by orders of magnitude (Edwards, USAF Supercritical Hydrocarbon Fuels Interests). Atomization of liquid fuels during fuel injection relies on viscosity and surface tension as well as the density ratio between the fuel and air to achieve efficient combustion. As the fuel becomes supercritical, all these values change making the behavior of supercritical fuels difficult to understand.

At supercritical conditions, endothermic reactions may occur. An endothermic reaction absorbs heat as the bonds within the compounds are broken. This chemical reaction (thermal cracking) produces lighter hydrocarbons and hydrogen (Huang, 2004). Although a fuel has yet to be used in this manner within a working system, the amount of heat that an endothermic fuel may be able to absorb would be significant. A plot of the approximate heat sink values attained for different jet fuels over decades is shown in Figure 1 below.

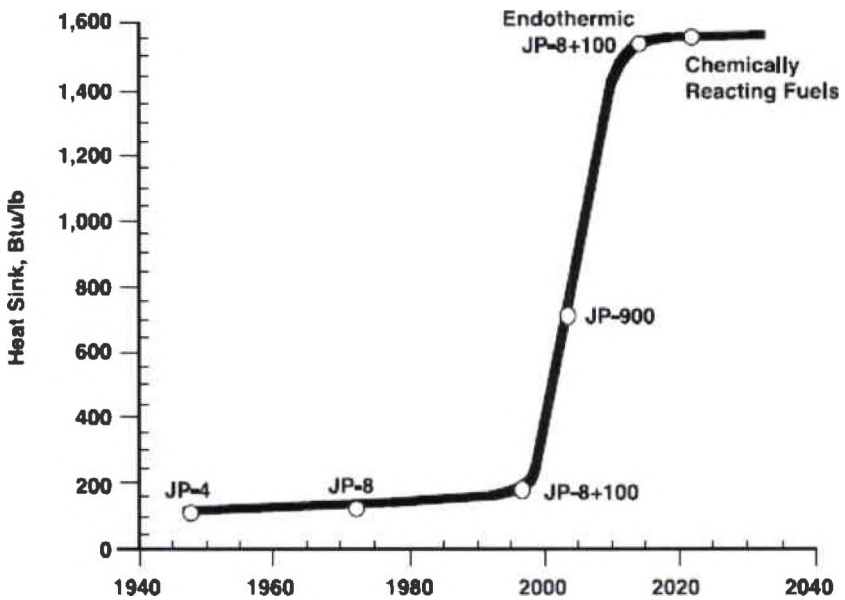

Figure 1: Increase in Heat Sink of Jet Fuels
(Macdonald, USAF Scientific Advisory Board)

With respect to heat sink, Figure 1 shows that endothermic fuels have a large advantage over their conventional counterparts. Hindrances in the use of endothermic fuels include the potential for thermal oxidation at low temperatures and pyrolysis as temperatures exceed the critical temperature.

1.2 Thermal Oxidation and Pyrolysis

Thermal oxidation is a process in which a hydrocarbon fuel reacts with the oxygen dissolved within it in the presence of heat. Thermal oxidation typically begins to occur at a temperature of 140°C (Striebach and Rubey, 1994). This series of reactions results in soluble gums and insoluble surface deposits. The surface deposits can restrict fuel flow within fuel lines and cooling passages, and decrease heat transfer in heat exchangers. Fuel injector nozzles and fuel filters can become blocked by surface deposits. If the deposits accumulate over long periods, they may cause engine damage. The formation of peroxides and hydroperoxides during thermal oxidation can damage elastomeric fuel system components such as O-rings (Chevron Products Company, 2000).

Pyrolysis begins to occur at temperatures (approximately 450°C) higher than those of thermal oxidation when the oxygen in the fuel has been consumed (Ervin, 2003). Pyrolysis is a chemical process where the bonds of hydrocarbon molecules are broken to produce several smaller molecules (Ward, 2004). A hydrocarbon fuel has a tendency to break down into smaller carbon number alkanes and alkenes as well as other products. These products can form surface deposits much like thermal oxidation and cause similar problems in an engine.

1.3 Influence of Heating on Flow Field within a Tube

Both experiments and numerical simulations are used to improve understanding of jet fuel behavior. Thermal stability testing is often performed by flowing fuel through a heated tube (Katta, 1995). The conditions used to heat a fluid are important for thermal stability experiments and simulations. Because a secondary use of a fuel is as a coolant,

any study of fuel properties should include the heating of that fuel for deposition studies. Many experiments employ either an electrical current to the exterior of the tube or place a thermally conductive material around the tube and control the temperature of that material. In a computational fluid dynamics analysis, these boundary effects can be accomplished by applying numerical boundary conditions to the tube surface.

Heating flowing fuel in a horizontal tube influences the flow field. As the fluid near the wall is heated, the density decreases and the fluid there may accelerate due to buoyancy forces. The cooler and, therefore, higher density fuel at the tube center sinks due to gravity. This phenomenon may lead to a Kelvin-Helmholtz instability, which establishes two spiral vortices that are symmetrical about a vertical meridional plane (Katta, 1995). This combined forced and natural convective flow causes the heat-transfer coefficient to be higher than that predicted using laminar flow assumptions. Most studies which consider simultaneous forced and natural convective flow have been performed using large diameter tubes (>1 cm) (Katta, 1995). In smaller diameter tubes, the larger vortices resulting from Kelvin-Helmholtz instabilities break down creating a flow field similar to turbulent flow even though the Reynolds number is below 2300. As the mass flow rate increases, the inertial forces in the axial direction become dominant over the buoyancy forces. This situation favors the laminar model and the turbulent estimate becomes less representative. At a Reynolds number of 2300, the buoyancy forces become negligible relative to inertial convective forces in the flow and, beyond this point, the flow remains turbulent (Katta, 1995).

Because the flows within small-bore horizontal tubes can resemble a turbulent flow field even at lower Reynolds numbers, turbulent models have been used in past

numerical studies (Duangthip, 2004, Katta, 1995). These past simulations have been two-dimensional and axisymmetric. The advantages of this two-dimensional approach for modeling the flow field are that it allows for the use of a small mesh size and simple meshing. However, the two-dimensional model cannot simulate the effects of buoyancy and the instabilities formed when heating. To examine the effects of these forces and instabilities in the tube, it is necessary to have circumferential gradients and to use a three-dimensional model.

The non-rotating model is useful for fuel thermal stability tests; however, there may be further interest in rotating flow. The flow in a rotating tube can be broken down into primary and secondary flow components. The primary flow can be defined as the axial flow and the secondary flow as the flow effects induced by tube rotation. As the rotational velocity increases, the axial flow decreases and flow resistance increases. If the centripetal acceleration and translational acceleration are considered to be hydrostatic, the vorticity of the secondary flow is caused largely by the Coriolis acceleration. The secondary flow is symmetrical about the diameter located at $\theta = 90°$ so that fluid particles in the plane passing through this diameter tend to remain in that plane (Morris, 1981). Heating the tube results in the centripetal acceleration and translational acceleration not remaining hydrostatic and creating the centripetal-type buoyancy already discussed in addition to the vorticity generated by the Coriolis acceleration.

1.4 Objectives

The primary focus of this thesis is to further the understanding of the fluid dynamics and heat transfer of JP-10 in a gravity field. The chemical structure of this fuel is exo-tetrahydrodicyclopentadiene (tricyclo[5.2.1.$0^{2,6}$]decane) and is essentially a pure

substance. This fuel has the possibility of being used as an endothermic fuel at supercritical conditions. The goal is to simulate the flow of JP-10 in normal gravity within a heated horizontal straight tube. Next, a higher gravitational field will be imposed by a rotational acceleration. Both of these kinds of simulations will be reformed using a three-dimensional model instead of two-dimensional axisymmetric model representations. A third experiment will be designed to determine if the gravitational field from a rotational acceleration can drive fuel into a heated tube and if when heated the buoyancy drives the fuel against the rotation induced gravity. This experiment will use both a two-dimensional axisymmetric and a three dimensional model.

The fuel moving through a horizontal straight tube will be simulated at supercritical and liquid phases. By simulating both phases, the affects of the temperature difference and phase change in the two different cases can be compared. This will be followed up by flow through a U-shaped tube. The flow will be examined in the supercritical and liquid phases as it moves around this bend. The U-tube will then be rotated. The main purpose for shaping the tube this way is to be able to better observe the fuel when a rotational acceleration is applied. In a straight tube, the fuel would flow out making it difficult to see the gravitational field applied by the rotational acceleration. This too will be done in both supercritical and liquid phases.

Finally, a rotating disk was designed to avoid pumping the fuel and instead allowing the rotational acceleration to force the fuel into the ends of the disk. After the fuel had entered the disk, heating the walls should generate buoyancy forces that attempt to force the fuel back out of the disk. The disk was designed with two internal flow paths along the outer walls and a bridge between these two flow paths. These flow paths were

attached to a tube running through the center of the disk. The fuel could be pumped into the tube and the effect of centrifugal force on the fuel could then be observed. Figure 2 shows a half slice of the disk. The fuel enters the left end of the tube and exits via the pressure outlet on the right end. Table 1 gives an overview of the simulations performed.

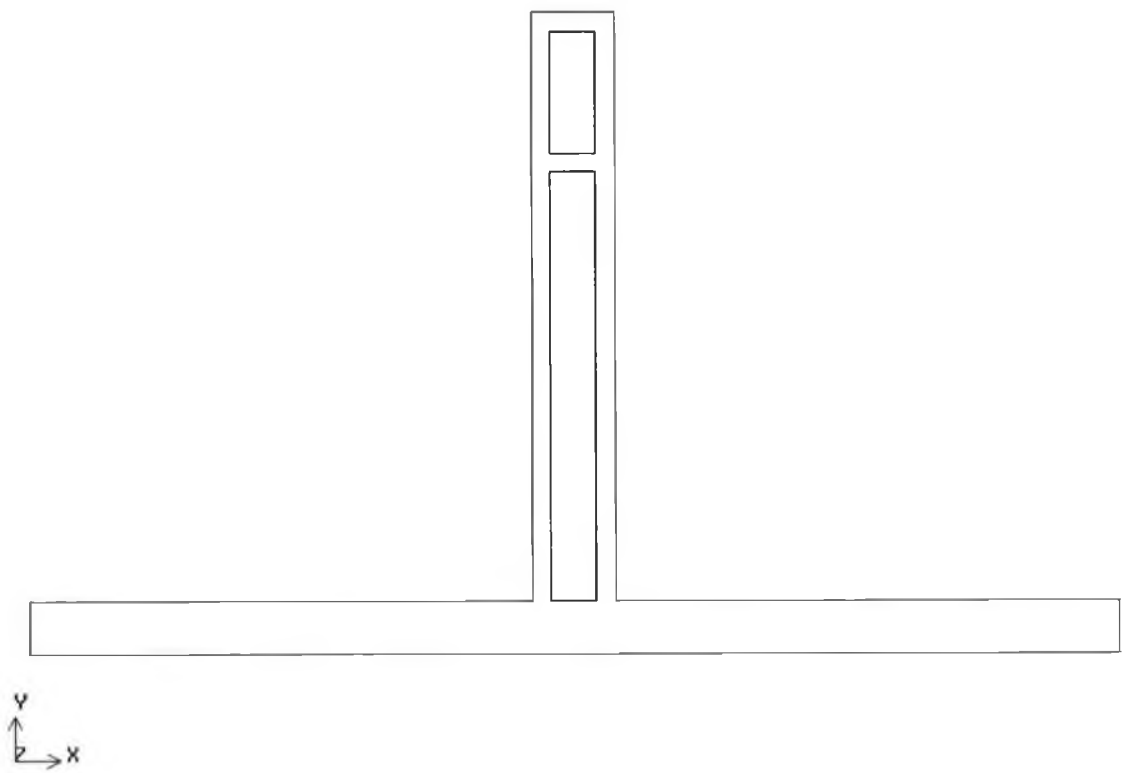

Figure 2: Cross Section of Rotating Disk

Table 1: Summary of Simulations Performed

Test	Description
Straight Tube	This simulation was performed in both liquid and supercritical phases. The primary use was to show the presence of buoyancy forces.
U-tube	The flow through this U shaped tube was simulated in both liquid and supercritical phases. The primary use was a first step toward testing heated fuel undergoing a rotation.
Rotating Disk	The disk was designed to investigate flow movement due to rotation and buoyancy forces. Fuel was not forced through the rotating section as it was in the U-tube. Simulations were attempted in the supercritical regime.

CHAPTER 2

NUMERICAL METHODOLOGY

2.1 Thermodynamic Properties

The CFD program used here for the simulations is Fluent. Fluent is a commercially available program that has several different options for fitting the material properties of a fluid in the liquid phase including linear-piecewise and polynomial-piecewise fits, but all of these use temperature alone as the independent variable. The difficulty is with states that require both temperature and pressure to be specified as independent variables.

Fluent also has the capability to use user-defined functions for material properties. These functions require programming in C and using Fluent macros to create a user-defined function that can search a table of property values given the pressure and temperature of a grid cell. When the temperature and pressure do not match those values in the table, the program must interpolate between the two nearest temperatures and pressures. This table look-up has to be performed for every cell and iteration. Thus, time required for several hundred iterations can become excessive depending on how the user-defined function is written. Having a large number of thermodynamic properties in the table increases the size of the table and thereby increases computational time. Using a large number of temperature or pressure increments which determine the accuracy of the

table has the same effect. Therefore, accuracy and computational time both depend on the size of the table and the user must choose between a large, accurate table that requires much computational time or a less accurate table that reduces computational time. Another problem with using user-defined functions is that specific heat values cannot be entered into Fluent. This lack of flexibility prohibits the use of user-defined functions for the problem considered here.

Fluent has incorporated REFPROP, which is software that uses state equations with coefficients developed from experimental data. The National Institute of Science and Technology (NIST), the maker of REFPROP, has created a database file specifically for JP-10 to be used in REFPROP. The coefficients of the state equation were generated by NIST specifically for JP-10 to be used in the Helmholtz equation of state. The Helmholtz equation of state in REFPROP used available experimental data from the Fuels Branch of AFRL (Bruno, 2005). The limitations of this data were such that the number of terms in the equation of state used is only 10 compared to higher accuracy (0.01% to 0.1%) models that use 20 to 50 terms (Bruno, 2005). The Helmholtz equation is a combination of $a^0(\rho,T)$, the ideal gas contribution, and $a^r(\rho,T)$, the real gas contribution resulting from intermolecular forces (Equation 1). The real gas contribution (Equation 2) uses ten coefficients:

$$a(\rho,T) = a^0(\rho,T) + a^r(\rho,T) \tag{1}$$

$$\begin{aligned} a^r(\delta,\tau) = {} & n_1\delta\tau^{0.2} + n_2\delta\tau^{1.15} + n_3\delta^2\tau^{1.42} + n_4\delta^2\tau^{1.65} + n_5\delta^4\tau \\ & + n_6\delta^3\tau^{2.0}\exp^{-\delta} + n_7\delta^3\tau^{1.69}\exp^{-\delta} + n_8\delta^6\tau^{0.95}\exp^{-\delta} \\ & + n_9\delta^6\tau^{1.72}\exp^{-\delta} + n_{10}\delta^4\tau^{2.5}\exp^{-\delta^2} \end{aligned} \tag{2}$$

where $\delta = \rho/\rho_c$ and $\tau = T_c / T$ and ρ_c is the critical density and T_c is the critical temperature.

The coefficients, n_m, were determined by fits to the available experimental data. The data points were individually weighted according to type, region, and uncertainty (Bruno, 2005). The coefficients are listed in Table 2.

Table 2: Coefficients of the Real Gas Contribution to the Equation of State

m	n_m
1	1.64044
2	–2.75277
3	–1.04100
4	0.909461
5	0.0396564
6	–0.429241
7	1.21962
8	0.0609974
9	–0.0798114
10	–0.0439556

Modeling a phase change from a compressed liquid to a supercritical fluid in Fluent adds complexity to the present simulations. This complexity leads to longer convergence time and inherent difficulties in finding a converged solution. We avoid sudden changes in thermodynamic states as the fluid goes from compressed liquid to supercritical fluid. Figure 3 shows this liquid to gas phase change "dome" between the 625 K and 700 K isotherms. If a pressure above the critical pressure of 3.733 MPa is modeled, the fluid goes from compressed liquid to supercritical fluid as the temperature increases.

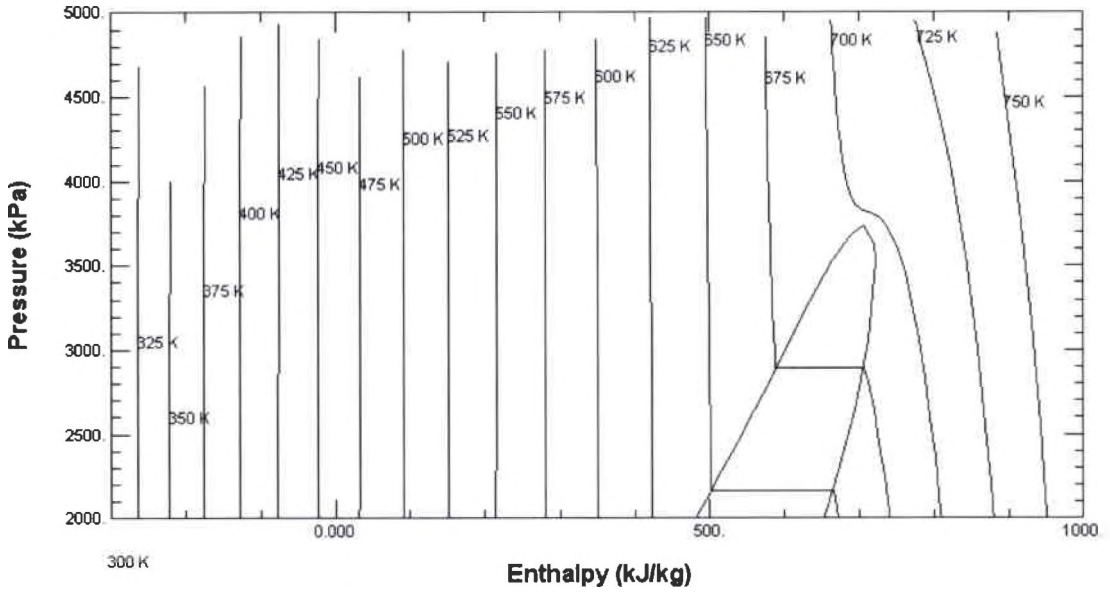

Figure 3: Enthalpy - Pressure Diagram for JP-10

2.2 Governing Equations and Models

The governing equations for a three-dimensional model in this commercial software program are:

$$\frac{\partial \rho}{\partial t} + \nabla \cdot (\rho \vec{v}) = S_m \tag{3}$$

$$\frac{\partial}{\partial t}(\rho \vec{v}) + \nabla \cdot (\rho \vec{v} \vec{v}) = -\nabla p + \nabla \cdot (\bar{\bar{\tau}}) + \rho \vec{g} + \vec{F} \tag{4}$$

$$\frac{\partial}{\partial t}(\rho E) + \nabla \cdot (\vec{v}(\rho E + p)) = \nabla \cdot (k_{eff} \nabla T) + S_h \tag{5}$$

where ρ is density, $\vec{v}$ is velocity, S_m is mass source, t is time, $\vec{g}$ is gravity, $\vec{F}$ represents external body forces, E is energy, T is temperature, k_{eff} is the effective thermal conductivity, and S_h contains contributions from potential radiation and

volumetric heat sources. $\bar{\bar{\tau}}$ is the stress tensor defined as $\bar{\bar{\tau}} = \mu\left[\left(\nabla\vec{v} + \nabla\vec{v}^{T}\right) - \frac{2}{3}\nabla \bullet \vec{v}I\right]$ where μ is the molecular viscosity, and I is the identity matrix. Equation 3 is the continuity equation, Equation 4 is the momentum equation, and Equation 5 is the energy equation. Fluent uses the finite volume method, integrating the governing equations using infinitesimal control volumes to convert them to algebraic equations. These equations are used to model JP-10 flowing as a compressed liquid and at supercritical conditions.

2.2.1 Examining Fluent Using a Simple Supercritical Model

According to the Fluent manual (2005), liquids and multiphase flows are excluded from the NIST real gas model which would allow Fluent to access properties from REFPROP and use them in solving the governing equations. A simple test for Fluent's ability to handle a liquid and supercritical phase simultaneously was conducted using a meshed rectangle (Figure 4 below). JP-10 entered the left side and exited through a pressure outlet on the right side. The wall temperature was fixed at 730 K with an inlet temperature of 300 K. With an operating pressure of 4.75 MPa, the heat transfer from the walls ensured that the JP-10 was in the supercritical regime, given that JP-10 has a critical temperature of 698 K and a critical pressure of 3.733 MPa. The density determined at each cell center in Fluent was then compared to the density calculated separately by REFPROP at that specific temperature and pressure. The result was a maximum error of 0.003 kg/m^3. Essentially, Fluent was correctly interpreting the data received from REFPROP and when compared to REFPROP alone outside the CFD program it was within 0.003 kg/m^3. This difference is small enough to assume that

Fluent is reasonably accurate when handling a liquid and multiphase flow with the NIST real gas model.

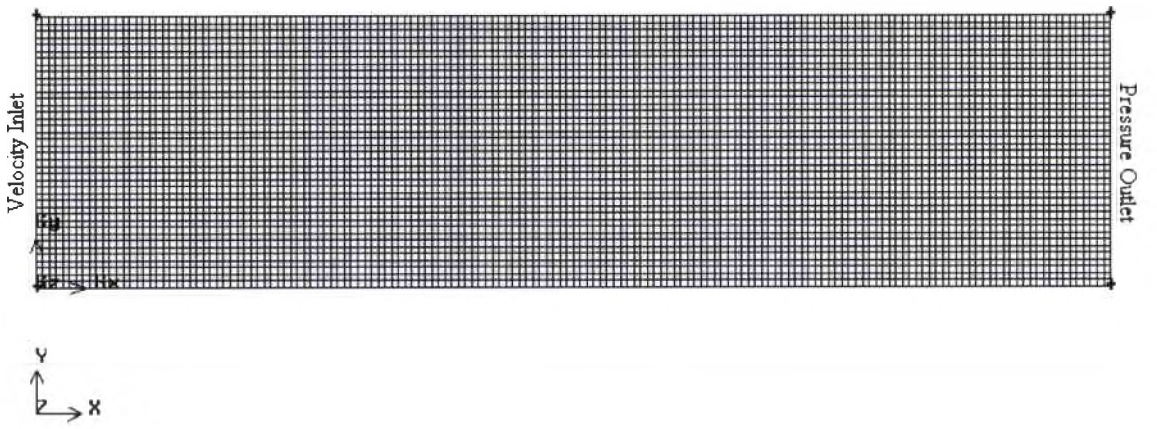

Figure 4: NIST Real Gas Model Rectangular Test Grid

Ultimately, the best option was not to use this model for the liquid phase test runs due to the extraordinary computational time penalty that accessing REFPROP incurs. A better option was to use the available temperature dependent linear piecewise model, which requires much less computational time. The temperature range for the heated liquid was from 300 K to 450 K. An interval of 10 K was selected such that 16 data points were used to partition this temperature difference for ρ, C_p, k, and μ. All of the data to make this piecewise linear model was taken directly from REFPROP.

2.2.2 Fluent and REFPROP Comparison

Four steady state test runs were performed to confirm the accuracy of the linear piecewise model. The runs were done using Fluent with a constant temperature of 315 K, 325 K, 355 K, and 425 K (Table 3). Grid size should not have much of an impact on this simple property test so it was maintained at a 6408 cell count structured mesh.

Table 3: Linear Piecewise Model Accuracy Simulations

Cell Count	Vin (m/s)	P (Pa)	Dia. (in)	Length (in)	Constant T (K)
6408	0.02526	101325	0.125	18	315
6408	0.02526	101325	0.125	18	325
6408	0.02526	101325	0.125	18	355
6408	0.02526	101325	0.125	18	425

The results from these tests are in Table 4. These tests were performed at 101,325 Pa, but the pressure should not affect the results of the tests because the model is primarily temperature and not pressure dependent. This is because the fluid is weakly compressible. Therefore, the fluid will not experience a significant density change. At a constant temperature then, a change in pressure will do very little to change the properties of the fluid. The differences are all less than one percent for density, specific heat, thermal conductivity, and viscosity. They all appear to be reasonably accurate for this application although the viscosity percent differences appear to be larger than the others are. While there is some uncertainty about why, this level of accuracy is acceptable.

The larger differences are in enthalpy and entropy, which are not shown in Table 4. However, these large differences are in fact not an error. The reason the differences are large and that there is a similarity between those differences is that the reference values for entropy and enthalpy are different for the two programs. These reference values or initial values make up the bulk of the discrepancy.

Table 4: Linear Piecewise Model in Fluent Compared to Values in REFPROP

Temperature	Fluent	REFPROP	% Difference
	Density (kg/m^3)		
315	918.0952	918.0955	3.27E-05
325	910.2252	910.2276	0.000264
355	886.3802	886.3838	0.000406
425	828.4952	828.5118	0.002004
	Specific Heat (kJ/kg-K)		
315	1.62183	1.621771	0.003638
325	1.663686	1.663643	0.002585
355	1.790811	1.790808	0.000168
425	2.086146	2.086168	0.001055
	Thermal Conductivity (W/m-K)		
315	0.110255	0.11026	0.004535
325	0.109105	0.10911	0.004583
355	0.10548	0.10548	0
425	0.096479	0.096479	2.07E-05
	Viscosity (mPa-s)		
315	0.020558	0.020447	0.541397
325	0.017449	0.017368	0.462482
355	0.011435	0.0114	0.306547
425	0.005519	0.005512	0.137809

2.3 Grid Generation for Straight Tube

The computational grid is very important for the solution of a problem. The accuracy of the solution hinges on the proper placement and number of cells in the model. Therefore, a careful grid selection process was used to determine whether the mesh would be valid. A Cooper mesh was used for both the U-tube and the horizontal tube. The Cooper mesh uses the grid on the face (the face perpendicular to the longitudinal axis of the tube) of the tube and stretches it across the length. The Cooper mesh scheme then sections the extruded mesh off along its length at a prescribed interval.

Using this ordered meshing method, the number of cells could therefore be altered in two directions, across the diameter and along the length.

The method employed for testing the grid was to use a rake, a line of points at equal intervals from one another, along the centerline of both the straight and U-tube. For the straight tube, the points in the rake were placed every inch starting at the velocity inlet and ending at the pressure outlet for a total of 19 points. The boundary conditions in Table 5, which shows all the runs for the straight tube grid analysis, were applied in Fluent for a steady-state solution. With a wall temperature of 450 K and a fuel inlet temperature of 300 K, there is heat transfer within the fluid and a temperature gradient. The points in the rake were used to measure temperature and the temperature at each point was then compared to those of the previous mesh. The mesh with the largest number of cells was assumed to be the most accurate and was used as a baseline for purposes of comparison. Given that the grid can be altered in the axial and radial directions, one of the directions was held constant, and the other was changed to determine how grid changes in a particular direction affects grid independence. The first three cell counts in Table 5 were used along the axial direction and the last four were used in addition to the 12816 run for the radial direction.

Table 5: Grid Evaluations Performed on Straight Tube

Cell Count	V_{in} (m/s)	P (Pa)	Length (in)	Constant Wall T (K)
6408	0.02526	101325	18	450
12816	0.02526	101325	18	450
25632	0.02526	101325	18	450
17136	0.02526	101325	18	450
22032	0.02526	101325	18	450
26784	0.02526	101325	18	450
31392	0.02526	101325	18	450

For all tube designs, the diameter of the tube requires at least ten cells across it to properly resolve the flow field. Therefore, the radial increment of cells was set at every 0.012 inches in order to have at least ten cells across the diameter while the axial cell increment was altered. The first axial increment was set at every 0.25 inches. This combination resulted in a total of 6,408 cells. Every proceeding interval was double that of the previous up to 25,632 cells. Table 6 below shows the data from each run and the difference from the largest grid of 25,632 cells.

Table 6: Results of Axial Grid Evaluation of Straight Tube

	Cell Temperatures			Temperature Difference from 25632	
Cell Number:	6408	12816	25632	6408	12816
Position (in)					
0	300	300	300	0	0
1	338.504	338.668	338.732	0.228	0.064
2	375.952	376.388	376.357	0.405	-0.031
3	398.576	398.74	398.718	0.142	-0.022
4	412.992	413.111	413.128	0.136	0.017
5	422.803	422.886	422.916	0.113	0.03
6	429.671	429.725	429.763	0.092	0.038
7	434.611	434.653	434.698	0.087	0.045
8	438.224	438.264	438.318	0.094	0.054
9	440.875	440.913	440.974	0.099	0.061
10	442.848	442.887	442.952	0.104	0.065
11	444.334	444.375	444.445	0.111	0.07
12	445.464	445.506	445.58	0.116	0.074
13	446.327	446.371	446.445	0.118	0.074
14	446.99	447.036	447.109	0.119	0.073
15	447.505	447.552	447.622	0.117	0.07
16	447.907	447.955	448.024	0.117	0.069
17	448.221	448.274	448.34	0.119	0.066
18	448.27	448.274	448.332	0.062	0.058

The temperature difference clearly decreases as the number of cells is increased along the length. At 12,816 cells, an interval of every 0.125 inches, the temperature difference becomes less than 0.1 K. This accuracy is acceptable for the simulations to be preformed in the straight tube. A difference this small will have little effect on the buoyancy forces under examination.

A similar analysis was done for the diameter. Holding the length interval constant at the selected 0.125 inches, the diameter was changed from the maximum interval of 0.012 to 0.008 in 0.001 intervals. The results of these variations in grid density are shown in the table below.

Table 7: Results of Radial Grid Evaluation of Straight Tube

		Temperature at Specified Intervals			
Interval:	0.012	0.011	0.01	0.009	0.008
Cell Count:	12186	17136	22032	26784	31392
Position (in)					
0	300	300	300	300	300
1	338.668	337.474	337.268	337.114	337.661
2	376.388	377.084	378.367	378.908	379.984
3	398.74	400.752	403.082	404.086	405.323
4	413.111	415.316	417.698	418.824	419.932
5	422.886	424.897	426.995	428.064	428.881
6	429.725	431.467	433.184	434.147	434.637
7	434.653	436.082	437.425	438.276	438.491
8	438.264	439.392	440.396	441.155	441.155
9	440.913	441.779	442.523	443.197	443.045
10	442.887	443.53	444.078	444.677	444.424
11	444.375	444.833	445.233	445.765	445.45
12	445.506	445.814	446.102	446.573	446.227
13	446.371	446.562	446.768	447.183	446.828
14	447.036	447.139	447.286	447.649	447.298
15	447.552	447.592	447.695	448.008	447.672
16	447.955	447.952	448.02	448.29	447.975
17	448.274	448.243	448.284	448.514	448.224
18	448.274	448.333	448.365	448.543	448.3

Using a diameter grid interval of 0.008 generates a grid of 31,392 cells. This grid was used as the baseline to compare the rest of the grids. The largest error is at the inlet of the tube (Figure 5). This is due to the larger temperature gradient there. The previously chosen grid of 12,816 cells is less than 2 percent difference from the grid of 31,392 cells. The grid of 22,032 cells is nearly less than half percent different from the 31,392-cell grid. This grid was chosen due to the accuracy and diminishing increase in accuracy for the additional 4,752 cells of the 26,784-cell grid. This grid was used for all the simulations using the 18-inch straight tube.

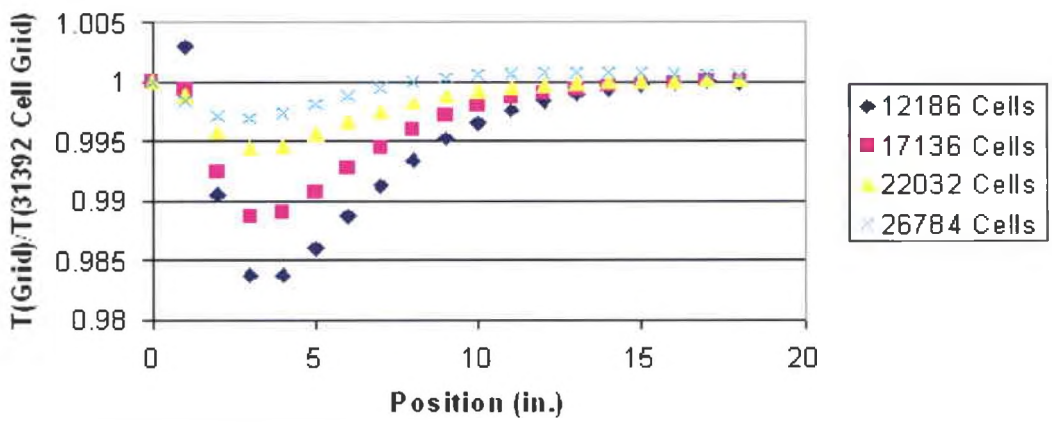

Figure 5: Grid Comparison of Smaller Cell Counts to 31392 Cell Grid

The five separate diameters have approximately 10 to 15 cells across the diameter (Figure 5). A hexahedral mesh was used instead of a tetrahedral mesh because tetrahedral meshes typically increase the number of cells, increasing the number of calculations and, therefore, increasing convergence time. Figure 6 shows the diameter of the tube after meshing.

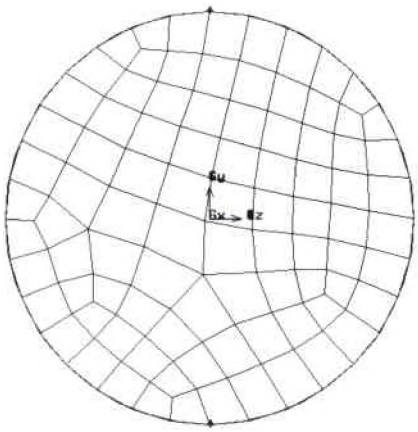

(a) 12816 Cells

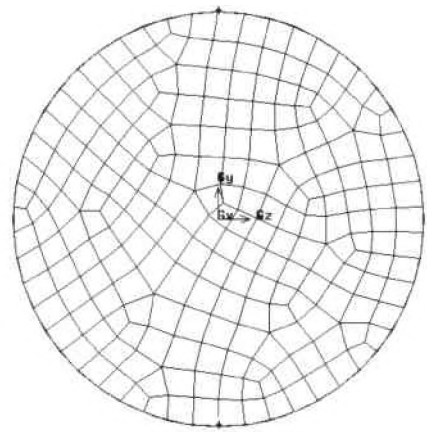

(b) 31392 Cells

Figure 6: Cells Across the Diameter of the Horizontal Straight Tube

Figure 6a shows the minimum number of cells across a diameter. This cell grid across the diameter was used for the 12816-cell test and all subsequent tests involving the straight tube. Because Figure 6 shows that there is an acceptable drop in accuracy with a decrease in cells across the diameter, the minimum number of cells could effectively be used to run all further tests.

The initial length of the tube was 18 inches but after observing the temperature gradient, 18 inches was determined to be unnecessary and the tube was shortened to 6 inches. Using the 18-inch grid took an extended period of time to converge and had a limited effect on accuracy. There was less than 2 percent difference in the diameter and 1 percent difference in the length. Thus, the 6-inch tube used a cell diameter interval of 0.125 inches to generate 10 cells across the diameter and a length interval of 0.25 inches. While not as accurate, the difference was acceptable, and this grid provided much faster convergence and allowed for easier use of Fluent features, such as animation.

2.4 Grid Generation for U-Tube

After creating a grid for the straight tube, it was necessary to generate a valid grid for the U-tube. The same Cooper meshing system and the same method for analyzing that mesh were used. To find the temperature for this model, a rake was placed every half inch along the 4.5 inches of the inlet and outlet sections. For the 1.5 inches outer radius bend, a point was placed every 15° along the center of the tube. The result was 10 points at each of the straight sections and 11 along the bend for a total of 31 points. Table 8 shows all of the runs performed while examining the U-tube grid.

Table 8: Grid Evaluation Cases for U-tube

Cell Count	V_{in} (m/s)	P (Pa)	Length (in)	Constant Wall T (K)
8262	0.02526	101325	12	450
16524	0.02526	101325	12	450
33048	0.02526	101325	12	450
12852	0.02526	101325	12	450
20088	0.02526	101325	12	450
23544	0.02526	101325	12	450

The procedure method was similar to that of the straight tube. The first three runs from Table 8 examined the lengthwise grid with the diameter held constant at an interval of 0.01. The diameter was held constant at this interval because the straight tube grid had had acceptable accuracy with this diameter interval. The table below shows the data from each run and the difference from the largest grid of 33,048 cells.

Table 9: Results of Axial Grid Evaluation of U-Tube

		Cell Temperatures			Temperature Difference from 33048	
Cell Number		8262	16524	33048	8262	16524
Position (in)						
X	Z					
0	0	300	300	300	0	0
0.5	0	314.485	310.187	308.477	-6.008	-1.71
1	0	336.611	336.374	336.482	-0.129	0.108
1.5	0	358.049	358.754	358.905	0.856	0.151
2	0	376.951	377.623	377.718	0.767	0.095
2.5	0	391.527	391.919	391.95	0.423	0.031
3	0	402.544	402.745	402.752	0.208	0.007
3.5	0	411.001	411.093	411.091	0.09	-0.002
4	0	417.629	417.667	417.66	0.031	-0.007
4.5	0	422.954	422.941	422.919	-0.035	-0.022
4.9	0.049	426.362	426.652	426.695	0.333	0.043
5.22	0.19	430.002	430.055	430.042	0.04	-0.013
5.52	0.42	432.336	432.671	432.699	0.363	0.028
5.74	0.72	434.755	434.742	434.76	0.005	0.018
5.89	1.07	436.198	436.499	436.53	0.332	0.031
5.94	1.44	438.075	438.102	438.154	0.079	0.052
5.89	1.81	439.144	439.529	439.586	0.442	0.057
5.74	2.16	440.727	440.79	440.829	0.102	0.039
5.52	2.45	441.554	441.912	441.961	0.407	0.049
5.22	2.68	442.899	442.935	442.976	0.077	0.041
4.87	2.83	443.503	443.842	443.88	0.377	0.038
4.5	2.93	444.482	444.614	444.659	0.177	0.045
4	2.93	443.863	443.798	443.771	-0.092	-0.027
3.5	2.93	443.861	443.779	443.799	-0.062	0.02
3	2.93	444.628	444.686	444.738	0.11	0.052
2.5	2.93	445.233	445.265	445.315	0.082	0.05
2	2.93	445.721	445.755	445.811	0.09	0.056
1.5	2.93	446.138	446.175	446.235	0.097	0.06
1	2.93	446.494	446.538	446.599	0.105	0.061
0.5	2.93	446.833	446.847	446.913	0.08	0.066
0	2.93	446.818	446.771	446.755	-0.063	-0.016

The largest grid temperature difference is at the entrance of the tube. At the cell position of (0.5, 0), there is a 6 K temperature difference from the 33048 cell grid to that of the 8262 cell grid. Again, this was expected due to the large temperature gradient as

the entering (300 K) fuel contacts the tube walls at 450 K. After the first half inch, the temperature differences among the grids are considerably less significant. The results used for the study of fuel as it moves through the U-tube will not be examined near the velocity inlet. Therefore, this value makes little difference in the interest of creating a grid for this problem.

The next step was to determine the effects of the diameter on the U-tube grid. Figure 8 shows the percent difference from the largest tested grid. The points with z values of 2.93 coincide with the outlet tube where the temperature is nearly constant and results in less difference. Initially, the larger grid of 20088 was decided upon to reach a higher order of accuracy. The U-tube design can be seen in Figure 7.

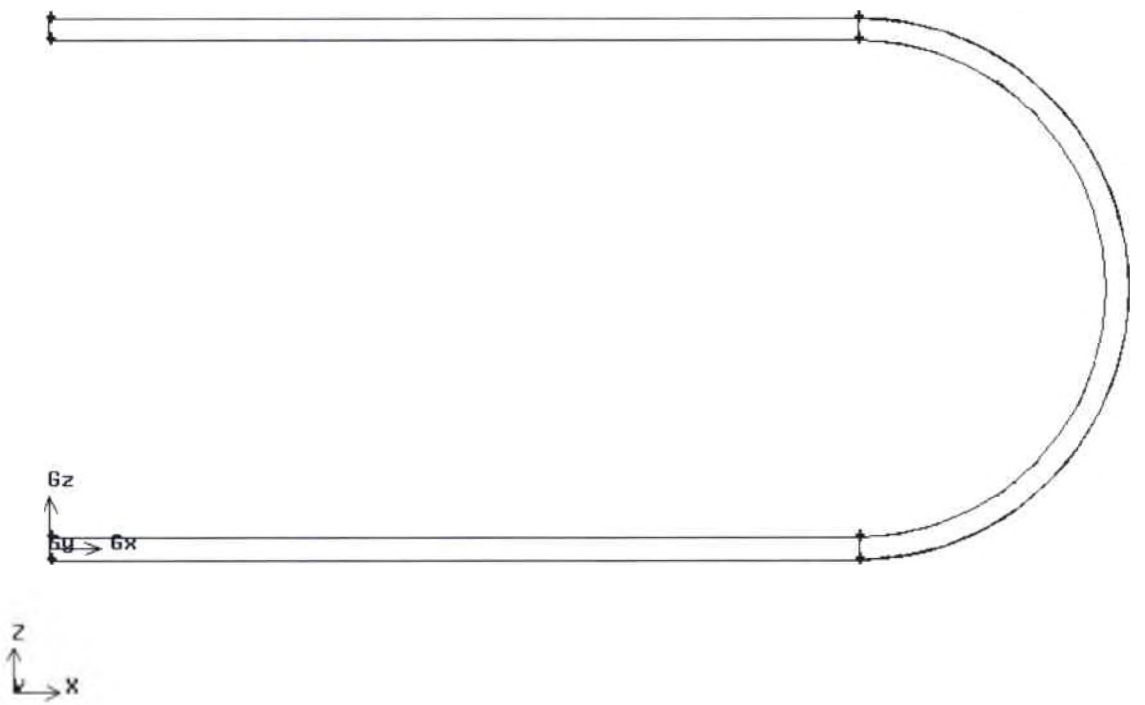

Figure 7: U-tube Design

The problems resulting from using such a large grid became clear when trying to reach a converged solution. Figure 8 shows that there is less than one percent difference

between the grids. The number of cells across the diameter can thus be taken down without much reduction in accuracy.

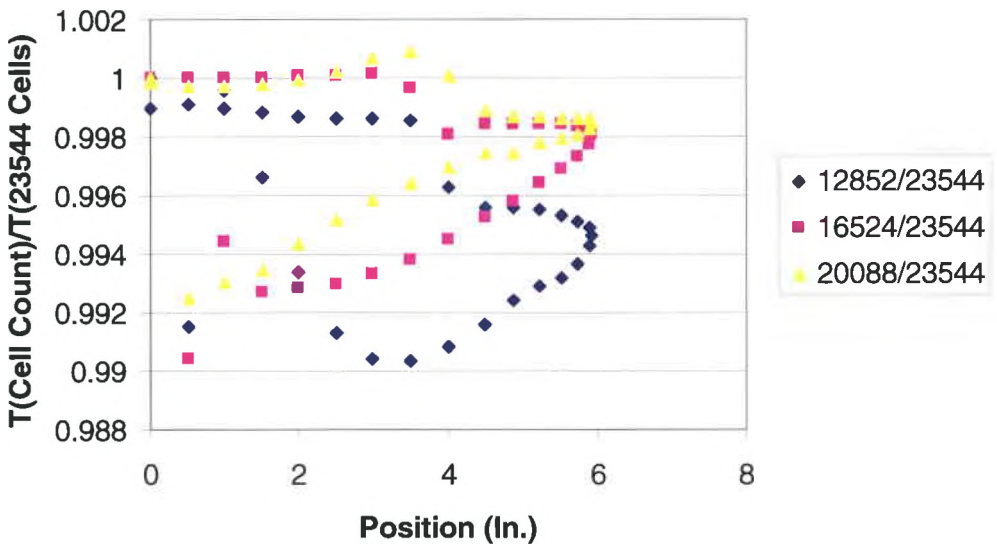

Figure 8: U-tube Diameter Grid Comparison

Ultimately, a much smaller grid of 3738 was used. This grid consisted of an interval of 0.125 across the diameter and length. The requirement for 10 cells across the diameter was then met while using as few cells as possible. The lengthwise interval of 0.125 corresponds to the same grid interval used for the 16524 cell grid. This means that the fuel near the velocity inlet will be less than 2 K in error rather than the rather large error of 6 K.

2.5 Compressed Liquid Fuel Simulations in the Horizontal Tube

The first simulations performed to explore the effects of buoyancy forces within flowing liquid JP-10 used the horizontal tube. This horizontal tube had a 0.125 inch inner diameter. This tube diameter is available for use in fuel thermal stability tests. The length of the tube allowed for the flow to become fully developed and for the flow exiting

the tube to reach the wall temperature. The initial tube length was 18 inches but after observing the temperature gradient, 18 inches was determined to be unnecessary and the tube was shortened to 6 inches. The wall temperature for the liquid phase simulation was set at 470 K, and the temperature of the fluid entering the tube was 300 K. This temperature difference will provide enough of a gradient to make the buoyancy forces detectable and allows the buoyancy forces to be observed at locations other than the entrance of the tube where the gradient is the largest. The inlet velocity was set at ~ 0.025 m/s, which is an approximation for the mass flow rate of 12 mL/min. This flow rate was later altered to 0.005 m/s in order to maintain the same Reynolds number at the inlet for both the supercritical and liquid tests. At the outlet, the supercritical test would exceed a critical Reynolds number of 2300 (the approximate value describing the transition from laminar to turbulent flow) and become turbulent. The pressure is set at 101,325 Pa. However, the operating pressure has a negligible affect on the results because the fuel is only weakly compressible. Finally, the gravitational constant was 9.806 m/s^2.

Given the temperatures at the inlet and outlet, an average density and viscosity could be found using REFPROP. An average Reynolds number could then be calculated. Table 10 gives property values used to define the Reynolds number.

Table 10: Reynolds Number for Liquid Fuel

	Inlet	Outlet
V (m/s)	0.005	0.005733
d (m)	0.003175	0.003175
ρ (kg/m^3)	932.81	813.56
μ (kg/m-s)	0.0028538	0.000476
Re	5.189	31.128

These Reynolds numbers are much less than 2300. Thus, the flow will be laminar. The solution of this simple problem proved rather difficult. The foremost difficulty was the initialization of the problem. The heat transfer resulting from convection and buoyancy, established vortices that change with time. An unsteady solution was necessary due to the transient behavior surmised to occur with the fuel. The local flow field resulting from convection and buoyancy should generate vortices that change with time. However, all standard initial conditions available in the Fluent initialization routine resulted in numerical divergence of the CFD solution. For this reason, all of the solutions were achieved by first solving the problem in steady state, which thereby provided an acceptable initial condition for subsequent unsteady analysis. All simulations used the 2^{nd} order implicit unsteady formulation.

The SIMPLEC (Semi-Implicit Method for Pressure-Linked Equations Consistent) algorithm was chosen for the solution of the steady problem (Fluent Inc., 2005). The under-relaxation factors were adjusted so that pressure was set at 0.7 and momentum at 0.3 with all other values at 1.0. To insure that the problem had been properly resolved, the solver was allowed 600 iterations. The algorithm was then switched to PISO and the under-relaxation factors were all set to 1.0. The PISO algorithm is recommended for transient flows by Fluent, Inc. and can maintain a larger time step than SIMPLEC. The segregated and implicit solver settings were used for this algorithm.

2.6 Supercritical Fuel in Horizontal Tube

The next step was to evaluate the buoyancy forces in JP-10 as it flowed in a supercritical phase. This simulation was also initially performed in the horizontal tube. The inlet velocity and temperature remain the same as those used for the liquid fuel test

for the supercritical fuel test. The wall temperature is increased from 470 K to 750 K, above JP-10's critical temperature of 698 K and the pressure is increased to 4.75 MPa, which is above the critical pressure of 3.733 MPa. The reason for setting the pressure much higher than the critical point is to avoid liquid to gas phase change.

The laminar model was used for supercritical JP-10 as well. Table 11 shows the Reynolds numbers for both the outlet and inlet assuming that the outlet temperature will reach the wall temperature. Refer back to Table 6 and the results show that the outlet temperature nearly reaches the wall temperature making this assumption valid. The Reynolds number remains below the turbulent regime and, therefore, the laminar model should be used when solving this problem.

Table 11: Reynolds Number for Supercritical Fuel

	Inlet	Outlet
V (m/s)	0.005	0.024205
d (m)	0.003175	0.003175
ρ (kg/m^3)	932.81	192.69
μ (kg/m-s)	0.0028538	0.000027977
Re	5.189	529.30

For the supercritical phase, the properties were obtained using the NIST Real Gas Model. With its implementation, temperature and pressure are read from each cell after every iteration, and the real gas model evaluates the thermodynamic properties of JP-10. The NIST Real Gas Model must use the implicit coupled solver. This solver, unlike the segregated coupled solver, solves the mass, momentum, and energy equations simultaneously. This coupled solver does not require a pressure correction step, which increases computational time. However, the need to access REFPROP during each iteration increases the overall time to convergence as opposed to using fluids already included in the Fluent material database. The coupled solver also limits the amount of

control the user has over solution convergence, as the only two variables available to be adjusted for the unsteady coupled implicit solver are the Courant number and the time step. The pointwise Gauss-Seidel scheme used by the coupled implicit solver should be unconditionally stable. This makes it possible to set the Courant number to a very high value for faster convergence.

2.7 U-tube Simulation Design

The U-tube simulations were not much different from those of the straight tube. The Reynolds number in particular is assumed to only be affected by slight changes in relative velocity due to the bend. Any vortices should not increase the relative velocity too far beyond the stated outlet velocity. The temperature difference from the inlet to the outlet for the U-tube is the same as that for the straight tube model. Therefore, the density and viscosity should be within the same range of values. All of this implies that the Reynolds numbers will be within the same range as well and that the laminar model can be used for the U-tube.

The rotating U-tube is expected to generate vortices even without heat transfer. The size and direction of these vortices cannot be known a priori. However, it was anticipated that, in the absolute reference frame, the U-tube would have a significantly increased fluid velocity. At 20,000 rpm, the velocity at the outer radius of the U-tube bend would be approximately 320 m/s. This increases the Reynolds number too far above 2300 implying that the flow will be turbulent. However, this initial estimate was proven false. The velocity must be observed from relative reference frame in which the fluid is still moving at similar velocities to those when not rotating. Therefore, the

Reynolds number within the tube is actually very similar to those for the U-tube without rotation. The laminar model was consequently used again for the rotating U-tube.

Up until this point in the work, the simulations had been performed first by solving the problem in steady state to generate a good initial condition for the unsteady solver. This technique was unnecessary for the rotating simulations. In fact, switching between the two would often result in divergence. Given the solvers limited adjustment capabilities using the NIST Real Gas Model and an unsteady solver, the best option was to alter the time step size until the solution appeared to converge.

2.8 Rotating Disk Simulation Design

The initial design of the rotating disk was as an axisymmetric structure. This made it much simpler to design and mesh. A coarse mesh was used in order to provide a quick analysis of the fuel's movement through the rotating model. The model was initially run with air as the fluid to get a feel for the possible results and then later runs were attempted with decane, which could approximate the properties of JP-10. The velocity inlet was set at 0.005 m/s and the operating pressure was 4.75 MPa. The rotation was maintained at 2000 rpm, as this was a rotational velocity that could be achieved easily and still provided the forces due to gravity. Although these forces would not be as strong as those at 20,000 rpm, this solution was much easier to achieve.

A temperature difference had to be applied to examine whether or not buoyancy would cause the fluid to leave the disk and return to the straight tube. A boundary condition of 900 K was placed on the walls at and above the bridge, a temperature of 600 K was used at the inlet and outlet of the disk, and a temperature of 300 K was used in the straight tube. This created a second method for investigating the flow. The temperature

at the outlet of the straight tube should increase if the fluid actually entered and exited the disk.

Referring back to Figure 2, this model had a structured mesh applied to it to form an axisymmetric model used to examine the fluid's movement. The mesh maintained four cells across the disk area but this was later determined to be not enough to assure that the flow would be properly resolved. The mesh was changed from 4 cells to 10 cells across the area of the disk for the three dimensional model.

The next step was to create a full 360-degree model of the rotating disk in three dimensions to see if any changes occurred in the fluid's movement. Taking advantage of the inherent symmetry of the geometry, in order to reduce model cell-count, a quarter of the disk with periodic boundaries was used instead of the full 360-degree model. The grid size was 19961 cells in an attempt to maintain accuracy without increasing convergence time to an unreasonable degree. The mesh can be seen below in Figure 9 and Figure 10.

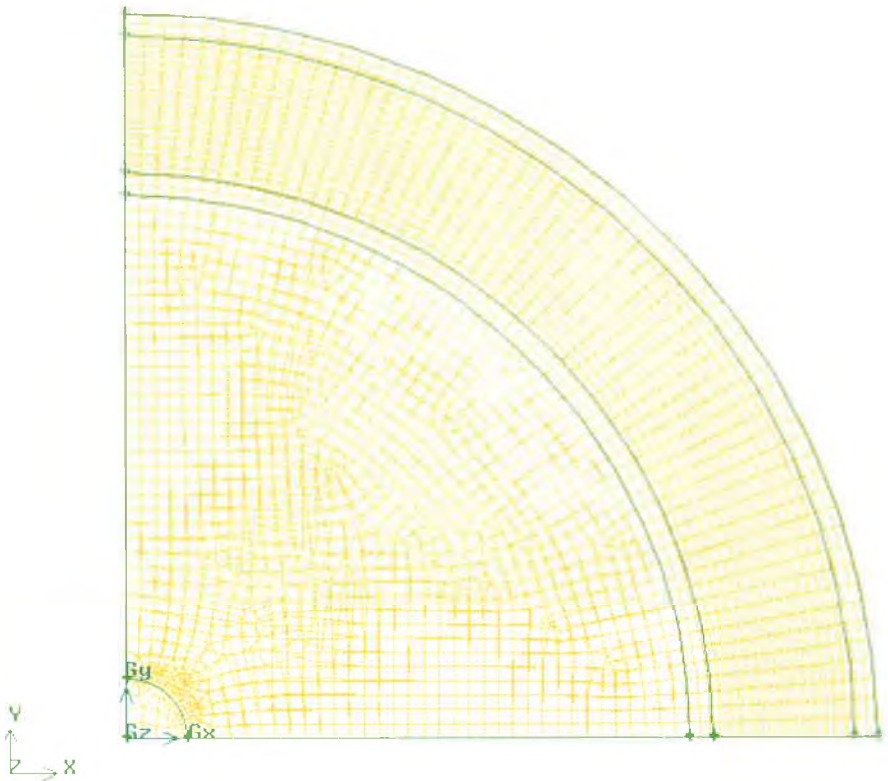

Figure 9: Velocity Inlet View of Rotating Disk

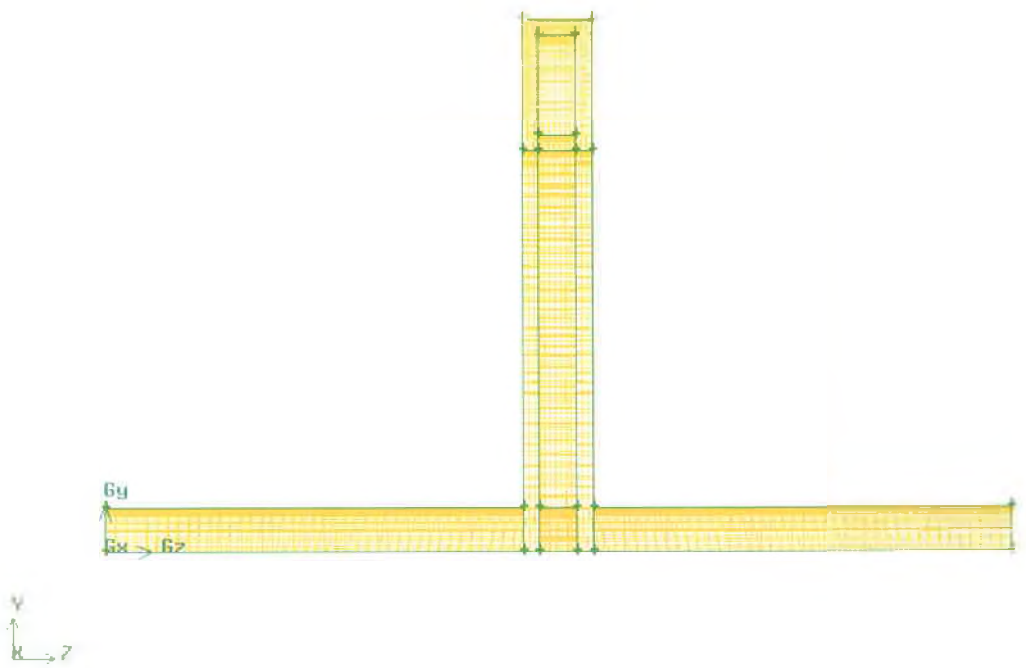

Figure 10: Side View of Rotating Disk

This mesh was less structured than the axisymmetric model. A Cooper meshing scheme was used on the straight tube and the areas of the disk, however, given the pie shape a pave mesh had to be used. The only other option would have been to use tetrahedrals, which would have increased the cell count and thereby increased the convergence time.

After this initial design was tested several times, the convergence problems became apparent. There was a strong possibility that the mesh was not fine enough to resolve the vortices and fluid movement through the smaller disk internal flow passages. As previously mentioned, the disk area was changed from a mesh of 4 cells across to that of 10 cells. This drastically increased the cell count to 67,455, over 3 times the size of the previous mesh. This also radically increased convergence time.

CHAPTER 3

RESULTS AND DISCUSSION

3.1 Overview

The appearance of buoyancy forces via the y-velocity was the focus of the cases without rotation. This was done to ensure that Fluent exhibited these forces. In the cases with rotation, the focus was on evidence of the flow's rotation and examination of the relative velocity. The relative y-velocity also allowed for examination of the buoyancy forces. The straight and U-tube have results for both liquid and supercritical fuel while the rotating disk only has test runs for air. The ultimate purpose of the rotating disk tests was to use the rotation and the gravitational field it creates to pull the fluid into the disk and the buoyancy force to drive the fluid out again.

3.2 Straight Tube

Table 12 shows the conditions for the simulations performed on the straight tube in the compressed liquid phase. As previously described, the straight tube was initially created with 22,032 cells. This cell count level and length proved to be unnecessarily high and both the cell count and length were reduced. The liquid phase was increased from a wall temperature of 450 K to a wall temperature of 470 K in the hopes that the larger temperature difference would make the buoyancy forces even more apparent.

Table 12: Compressed Liquid Simulations for Straight Tube

Cell Count	Vin (m/s)	P (Pa)	Length (in)	Constant Wall T (K)	Comment
22032	0.02526	101325	18	450	
2136	0.01	4750000	6	470	1% V_{in} fluctuation boundary profile at 1 Hz
2136	0.01	4750000	6	470	2% V_{in} fluctuation boundary profile at 1 Hz
2136	0.005	4750000	6	470	

All straight tube runs were transient due to the changes in the fuel imposed by the applied heat. Without the need to access REFPROP, the liquid fuel simulations were able to converge rapidly compared to the supercritical fuel simulations. Therefore, the simulations on the liquid fuel were run first and provided some insight into what to expect from further runs with the supercritical fuel even though there would be differences in the results. Given that these forces would be the focus of all other simulations, this simple test was essential. It is important to understand the flow in this configuration as well because it has relevance for thermal stability tests.

The supercritical fuel tests are shown in Table 13. The temperature has been increased from 470 K to 750 K. The velocity inlets and pressures are the same for both so that they can be readily compared and still maintain distance from the liquid to gas phase change.

Table 13: Supercritical Simulations for Straight Tube

Cell Count	Vin (m/s)	P (Pa)	Length (in)	Constant Wall T (K)
22032	0.01	4750000	18	750
2136	0.005	4750000	6	750

The inlet temperature was set at 300 K. The temperature difference of 170 K for the liquid fuel was large enough to generate small but observable buoyancy forces. The buoyancy forces were primarily observed using a contour plot of the y-velocity. The x-velocity makes up more of the velocity vectors and therefore the velocity vectors display does not show these forces in a meaningful way. This plot of the 6 in straight horizontal tube can be seen in Figure 11 for the liquid phase and Figure 12 for the supercritical phase. These plots show that the fluid near the left and right sides of the tube has a positive vertical velocity and the flow near the center has a negative vertical velocity. This would indicate that the fluid is indeed affected by buoyancy. All the plots represent a solution at one second so that they all could be compared. The liquid fuel solution ran for up to 10 seconds but after 1 second no significant changes occurred in the temperature distribution. The supercritical solution used a time step of 0.0001 seconds and would have taken a long period to solve further. The liquid without the velocity inlet profile used a 0.001 second time step and the two with velocity profiles used a time step of only 0.01 seconds.

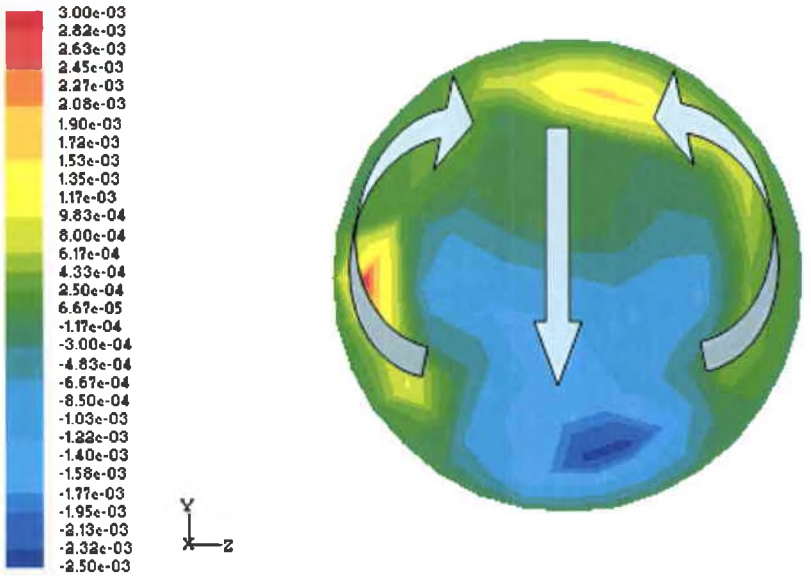

Figure 11: Y-Velocity of Liquid 1-inch After the Tube Inlet and After 1 second (0.01 time step)

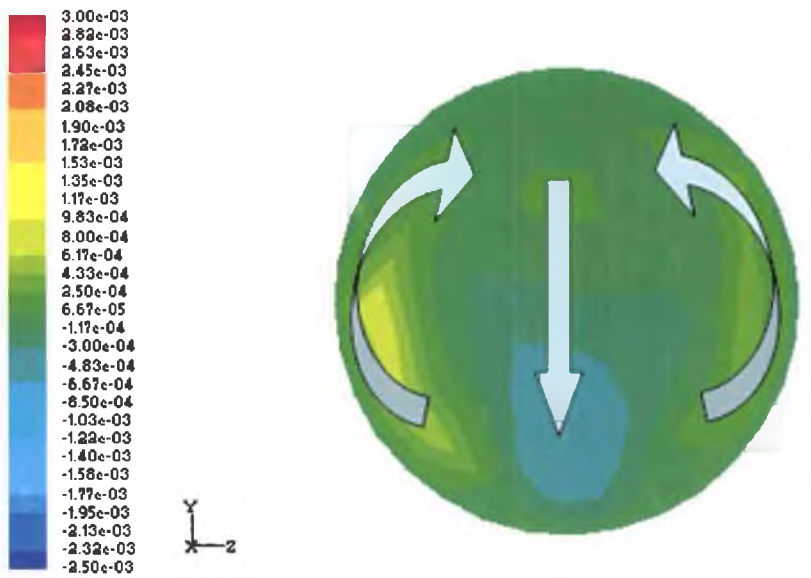

Figure 12: Y-Velocity of Supercritical 1-inch After the Tube Inlet and After 1 second (0.0001 time step)

Figure 13 and Figure 14 show a second contour plot of the static temperature for the liquid phase and supercritical phase, respectively. The temperature contour plots

serve to verify that the higher temperature and, therefore, less dense fuel rises to the top of the tube while the lower temperature, higher density fuel falls.

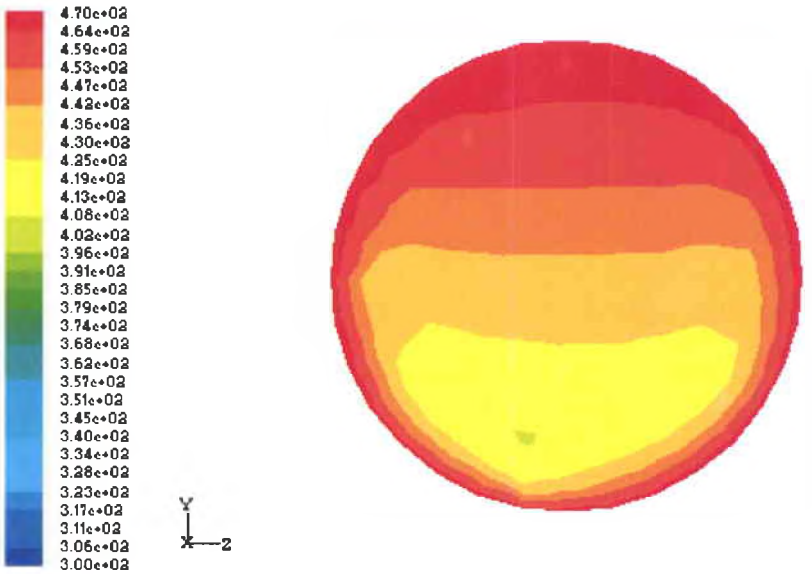

Figure 13: Temperature of Liquid 1-inch After the Tube Inlet and After 1 second

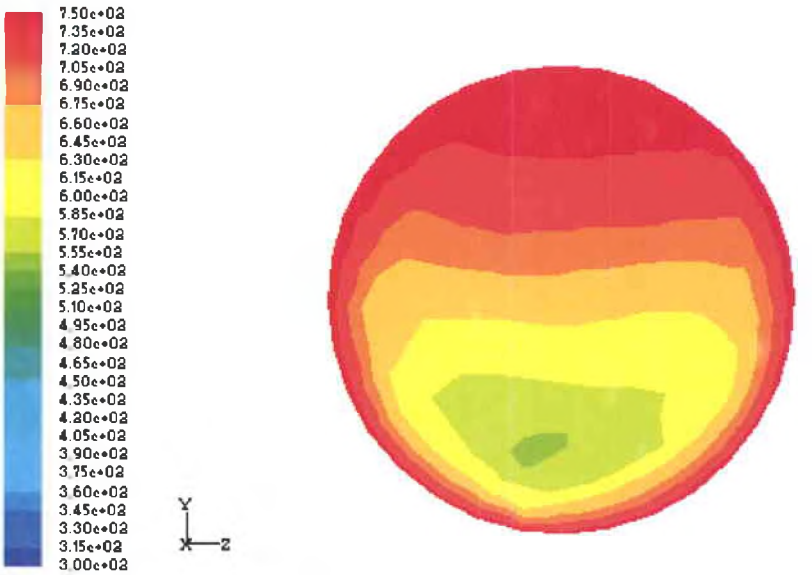

Figure 14: Temperature of Supercritical 1-inch After the Tube Inlet and After 1 second

The work of Katta (1995) indicated that a boundary profile that applied a frequency change to the velocity inlet was required to establish the Kelvin-Helmholtz instabilities. These runs were performed in two dimensions. The three-dimensional analysis did not require these same velocity inlet variations, however, simulations were performed at a frequency of half a hertz and a velocity fluctuation in amplitude of 1% and 2% of the initial velocity of 0.01 m/s. These simulations are shown below in Figure 15 and Figure 16. These figures were at 1 in from the velocity inlet.

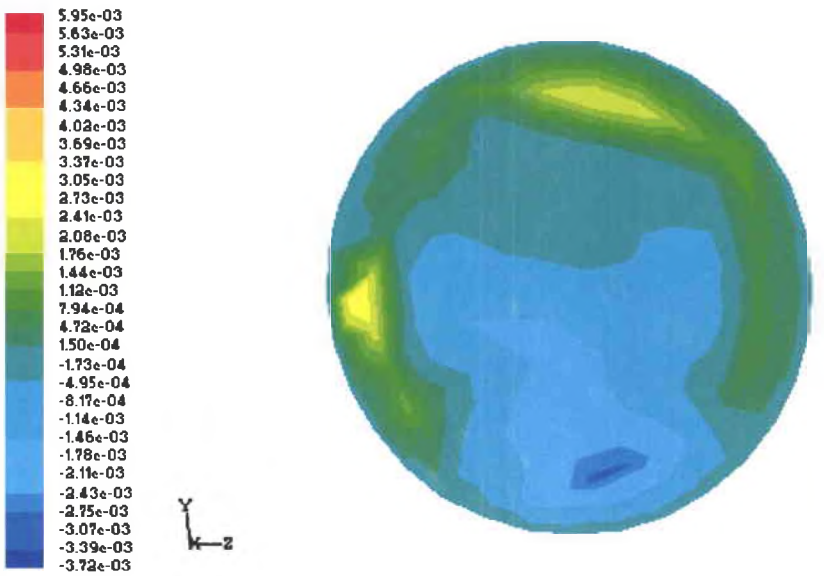

Figure 15: Y-velocity of Liquid Fuel with 1% Boundary Profile Applied at the Velocity Inlet 1-inch from the Velocity Inlet

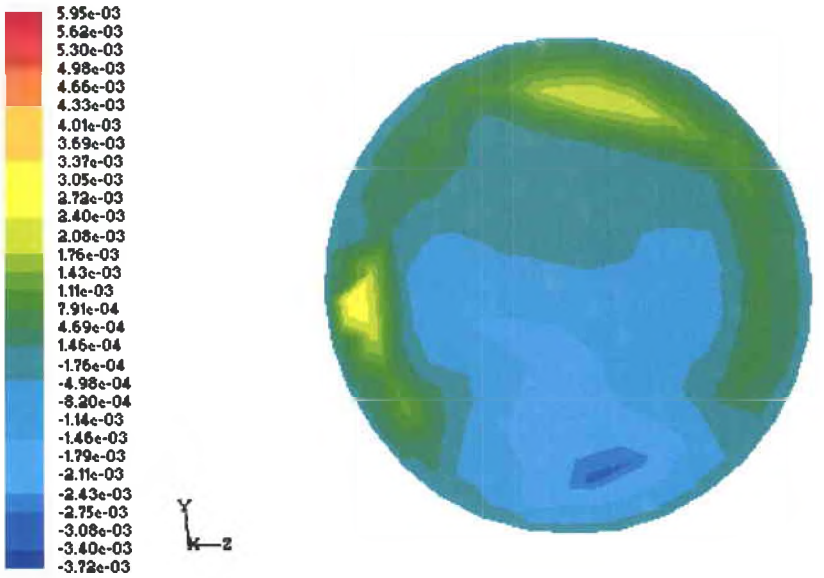

Figure 16: Y-velocity of Liquid Fuel with 2% Boundary Profile Applied at the Velocity Inlet 1-inch from the Velocity Inlet

The difference in the effects as far as the y-velocity is concerned seems to be negligible. The force is still present but there is not a large change that occurs from the introduction of a boundary profile. Another profile was introduced along the walls to examine the fluid as it underwent the change from 300 K to 470 K.

3.3 U-Tube

The U-tube case runs can be seen in Table 14. The primary focus was on obtaining a model that would be able to examine the supercritical fuel rotating.

Table 14: All Simulations Performed on the U-tube

Cell Count	Vin (m/s)	P (Pa)	Length (in)	Constant Wall T (K)	Comment
20088	0.02526	101325	12	450	Not Rotating
20088	0.02526	101325	12	450	Rotating at 2,000 rpm
9790	0.005	4750000	12	750	Rotating at 2,000 rpm
3738	0.005	4750000	12	750	Rotating at 2,000 rpm

After the grid examination, the initial U-tube model consisted of 20088 cells. The model was effective for both examining the liquid phase with and without rotation. The rotation case was only solved for 2000 rpm. The goal was to reach a rotational velocity of 20,000 rpm and according to the Fluent manual (2005), the starting should be around ten percent of the end value. However, attempting to start from 2000 rpm and ramp up to 20,000 rpm resulted in an error. Increasing the rpm from 2000 seemed to result in residuals beyond the point where they would begin to reach convergence again. The y-velocity for the not rotating U-tube can be seen in the figure below:

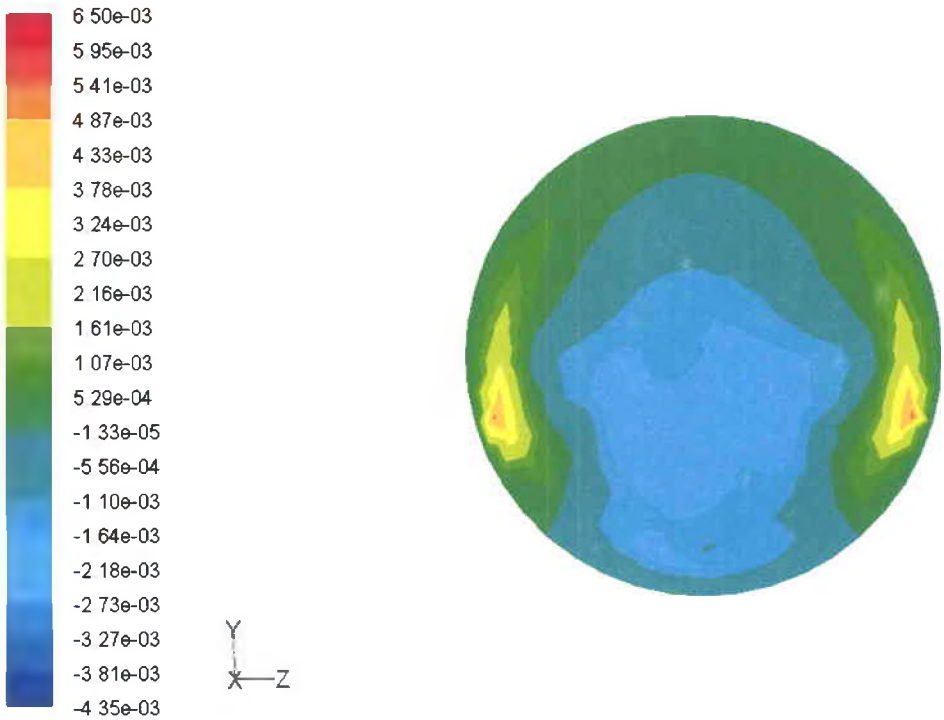

Figure 17: Y-Velocity 1-inch in U-tube after 1 second

The y-velocity again shows the temperature creates a buoyancy force. As the fuel reaches the temperature of the walls, the y-velocity disappears. This is a clear indication that the y-velocity is dependent on the temperature difference and therefore the buoyancy force.

The supercritical phase proved difficult to analyze using this model. The number of cells made it difficult to solve the problem in a reasonable amount of time due to a time step of 10^{-6} seconds that also had to be used to solve the problem. Accessing REFPROP at every iteration only served to further increase the time required for convergence.

To generate data on rotating tube cases, the liquid fuel was rotated at 2000 rpm. The desired speed was 20,000 rpm, however, there was a limit to which rotational velocity could be used. As rotational velocity was increased, the time step had to be

increased. This number of cells prohibited increasing the rotational velocity after start up even in the liquid phase. Rotational velocities beyond 10,000 rpm produced either an immediate error or an error within a few iterations. A rotational velocity of 2000 rpm was chosen to avoid these errors. This solution used a time step of 10^{-5} seconds and was allowed to run for 1 second.

The results of this run were used to analyze whether the simulation was set up properly and the fluid was indeed rotating. Figure 18 shows the velocity magnitude vectors at 3 inches into the U-tube inlet. The tube does appear to be rotating as the vectors are pointing perpendicular to the z-axis, axis of rotation. The color of the vectors indicates that the velocity magnitude lies somewhere between 14 and 17 m/s. The expected rotation velocity magnitude was hand calculated to be approximately 16 m/s. These values therefore appear to be valid.

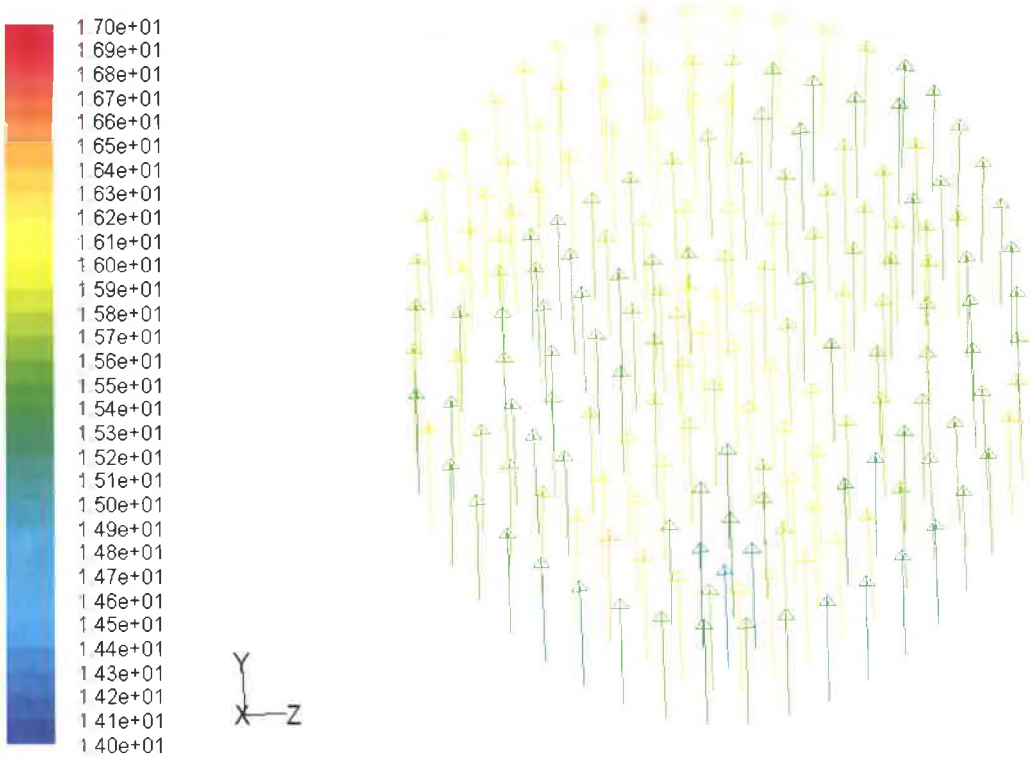

Figure 18: Velocity Vectors at 3 inches from Inlet

The relative velocity was also examined. Figure 19 shows the relative velocity vectors. The fluid in the lower half of the tube appears to moving toward the bend while the fluid near the upper half is returning toward the velocity inlet. This is most likely because not all the fluid is moving through the bend resulting in back flow.

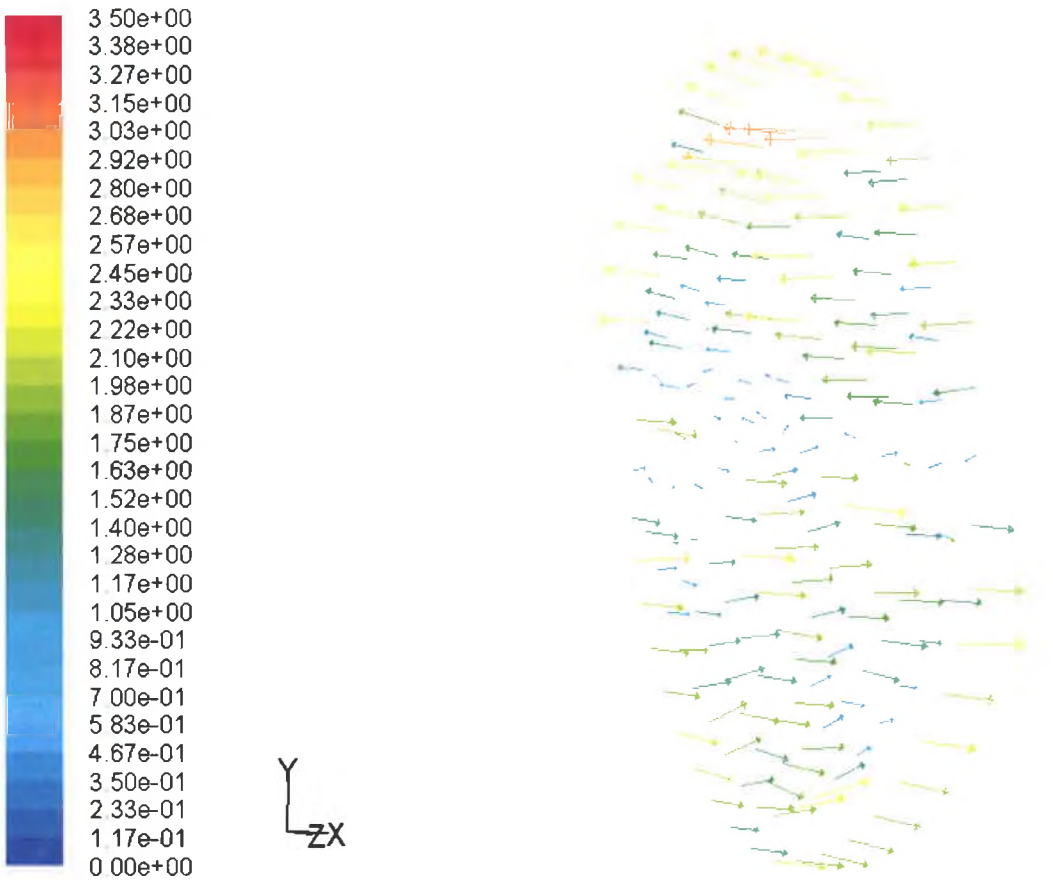

Figure 19: Relative Velocity Vectors at 3 inches from Inlet

The plane of vectors at the very center of the bend indicates that this is the case. Figure 20 shows this plane of vectors. The fuel in the bend appears to be a vortex with little of it moving around the bend of the U-tube. At this point in time, 1 second, the larger vectors indicate that the fluid is being pushed strongly against the upper portion of the outer wall.

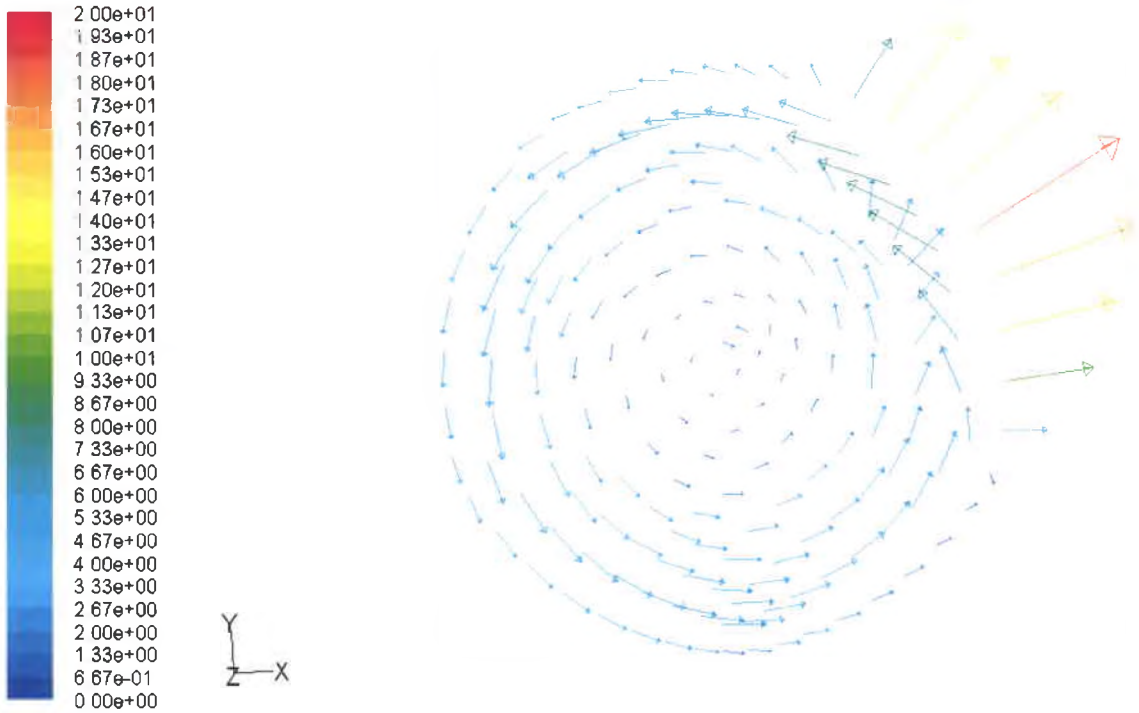

Figure 20: Vortex at the Bend in the U-tube

The next step was to use a coarser mesh in order to reduce the amount of time required for every iteration. The mesh was uniform along the inlet tube, bend and outlet tube and this was maintained for the 9790 cell model. The radial mesh remained the same size while the number of cells in the axial direction was reduced. This model was to be used specifically to examine the rotating supercritical fuel. Once again, the model started at 2000 rpm. Attempting to adjust the rotation speed from 2000 rpm to 4000 rpm resulted in divergence. After altering the rotational velocity several times, it became clear that the largest possible increase in rotational velocity was 100 rpm. Every 20 iterations at a time step of 10^{-6} seconds, the rotational velocity was adjusted by this value. While the solution continued to converge, this required the operator to be there every 20 iterations. In order to reduce the required time by reducing the time step and increasing the rotational velocity in larger increments, the cell count was again decreased.

This time the mesh was altered to reduce cells along the length of the inlet and outlet of the U-tube. It was necessary to have a more finely meshed bend so that the grid did not extend beyond the actual borders of the tube. The mesh was reduced to a cell count of 3738 cells. This cell count allowed the rpm to be increased in increments of 500 rpm until reaching 3500 rpm. At this point, the increment was reduced to 150 rpm for the solution to reach convergence. In addition, as the rotational velocity increased, the time step had to decrease to continue to have the solution converge. The time step started at 10^{-5} seconds and had to be decreased twice to 10^{-7} seconds by the time it reached 6650 rpm. At this time step, forcing a solution to convergence would take an untenable amount of time. There is also a good possibility that the time step would again have to be reduced at least once as the rotational velocity was increased toward 20,000 rpm. Ultimately, this made the solution of this problem intractable. In addition, the time step seemed to be required to decrease for the supercritical phase even when held at a constant 2000 rpm. The difference between the program's ability to solve the liquid and supercritical phase is probably related to the difference in the coupled and segregated solver. The segregated solver has a quite a few available control options and relies less on the size of the time step. While there is a possibility of finding an answer, the amount of time that would be required to reach 1 second with a time step of 10^{-6} would be extensive. There is also a possibility of requiring another time step reduction to reach a solution.

Even if a solution were to be found with this model, another problem exists. Pumping the fluid into the U-tube via the velocity inlet does not allow for examination of whether or not the fluid is forced into the tube by the rotation. Fluent does not have a

boundary condition that would not in some way force the liquid into the end of the U-tube. Therefore, the next course of action was to use a rotating disk configuration. The disk would have a tube through the center. The fluid within this tube would only have the force from the velocity inlet and the gravitational field from the rotation on it. In this way, the only method for the fluid to enter the disk would be from the force generated by the rotation.

3.4 Rotating Disk

The primary design of the rotating disk was to not pump the flow into the outer section of the disk but to prove that gravity would force the flow there and once there buoyancy would return the flow to the center tube. The results from the U-tube seemed to indicate that buoyancy forces were strong enough to force the flow toward the velocity inlet. These results made this experiment look conceivable.

As was stated previously, the mesh was kept rather coarse initially and solved in steady state. The coarse mesh had 4 cells across the width of the internal passage of the rotating disk. Ultimately, this was determined to be too coarse. The adjustment capabilities for the solver were limited primarily to the Courant number and the initialization procedure. In order to get convergence, the full multigrid (FMG) initialization method was used. This method essentially approximates the grid with an even coarser grid to provide an approximate solution and a better starting point for the solver. The Courant number was held low at the beginning to assure convergence and then increased to expedite convergence. However, it proved exceedingly difficult to force the residuals below 10^{-2} and 10^{-3} is usually considered the maximum residual value for a converged solution.

After getting the residuals to this point and being unable to force convergence any further, the results of the simulation were examined. Figure 21 shows that the results are incorrect. The fluid entering the tube through the left end of the tube reaches a higher temperature when the walls are maintained at the same temperature as the fuel.

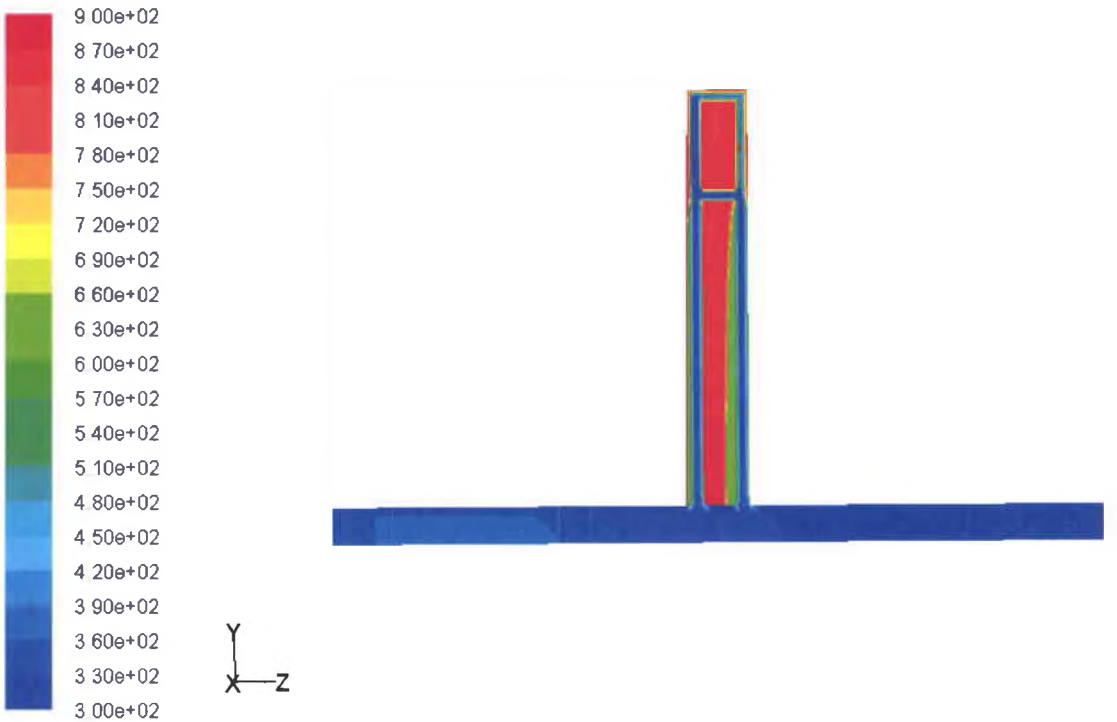

Figure 21: Temperature in the Coarse Mesh Model of the Rotating Disk

This error may be the result of the solution not being fully converged. There was also some concern over whether the flow inside the disk was being properly resolved by such a coarse mesh. To avoid this problem, the cell count was increased throughout the disk so that 10 cells were across the width of each internal flow path. In order to keep the cell count down, the center tube was decreased in size. The cell count increased from 19,961 to 67,455 cells.

However, the same problem existed for the fine mesh as it did for the coarse mesh. The residuals were again unable to be reduced below 10^{-2} and the results were

again incorrect. Figure 22 shows that the relative velocity vectors instead of moving out from the velocity inlet are actually headed toward it. This flow is at the center of the tube where there is little effect due to rotation. The flow should be moving to the right toward the pressure outlet.

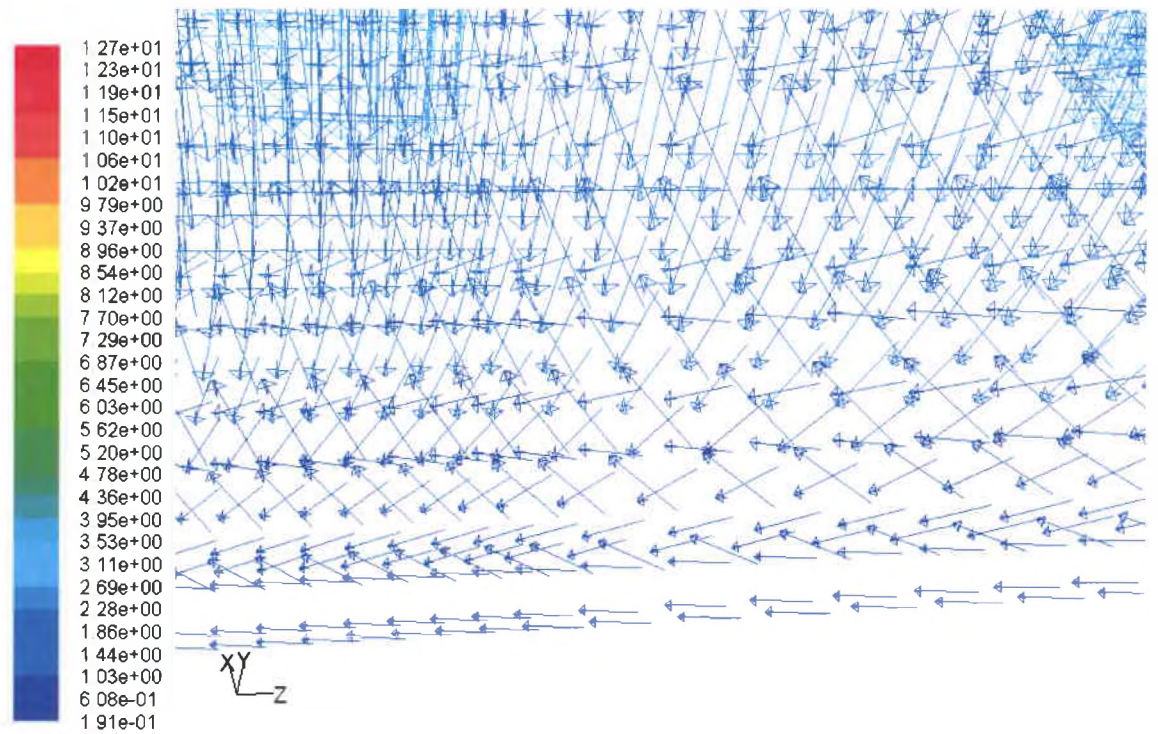

Figure 22: Relative Velocity Vectors Moving Toward the Velocity Inlet

The Fluent technical support office was unable to provide a valid solution for this problem. The solutions would not converge and the results were counter-intuitive.

CHAPTER 4

CONCLUSIONS

There were three designed simulations for this project. Each simulation had a specific purpose. The straight tube was designed to observe whether buoyancy forces were exhibited in Fluent. The U-tube was created to analyze the effects of rotation on the fluid and the rotating disk was intended to get a better look at the interaction between the buoyancy and gravitational forces. All of these models were three-dimensional and therefore were different than previous attempts to model similar flows.

Fluent showed that as the fuel was heated along the outer walls of the flow passage, with normal gravity imposed, the fuel near the walls became less dense. This was indicated by several cross sections showing density along the length of the tube. The y-velocity contour plots also indicated that the flow near the walls was moving against gravity while the flow in the center moved in the direction of the gravitational vector. This was the clearest indicator that Fluent correctly modeled the effects of buoyancy and could be used in further simulations like that of Katta's work (2005).

Katta designed a two-dimensional model for solving a very similar problem. This two-dimensional model required a boundary profile to fluctuate the mass flow rate at the

velocity inlet. This fluctuation created a necessary instability so that the solution would converge. In the three-dimensional model created here, the fluctuating boundary profile was proven unnecessary. Fluent was able to reach convergence without any alterations to the velocity inlet boundary profile and exhibited little influence from attempts at implementing such a boundary profile.

The U-tube results showed that the rotation in combination with the heat transfer set up several vortices within the tube. At the center of the bend, a vortex is created that rotates in the same direction as the entire U-tube. Along the straight sections of the U-tube, the fuel moves in opposite directions. At the top of the inlet tube, the fuel moves back toward the inlet, but at the bottom of the inlet tube, the fuel moves toward the bend. This vortex appears to be set up by gravity from the rotation forcing the fuel out toward the bend and heat from the bend creating buoyancy forces that push the flow back toward the inlet. There is also some pumping from the inlet that assist gravity to force the flow to the bend, while the buoyancy forces are assisted by the vortex near the center of the bend that slows movement of the fuel through the bend toward the outlet. These vortices were viewed via plots of relative velocity vectors. In addition to the vortices, the velocity magnitude vectors provided a check to the solution of this problem. The velocity magnitudes were hand calculated by converting rpm into m/s at various distances from the axis of rotation. The velocity magnitudes were then compared to the results in Fluent providing some confirmation that these results were correct.

These vortices showed that, in fact, the rotation was generating a force that pushed the fluid toward the bend. In turn, the buoyancy seemed to be acting against this

force just as it did against normal gravity in the straight tube simulation. This was the anticipated result of these runs.

The next simulation was to be used to further test these two forces. The design was such that the pumping would no longer be a factor in the results and the fuel would be influenced only by gravity and buoyancy. The hope was that it would enter the internal flow path on the inlet side of the rotating disk from the gravitational force and then exit out the other internal flow path due to the buoyancy force.

The rotating disk model had the grid design altered several times to increase the number of the cells and make it possible for Fluent to resolve the flow in the small width of the internal flow paths. Fluent has limited adjustment capabilities when using the NIST Real Gas model and therefore only the Courant number and initialization procedure could be altered. For each of these grids, multiple initialization procedures and changes to the Courant number were made. Unfortunately, convergence for this particular simulation was not possible. This meant that any solution put forth by Fluent would be inherently incorrect. This demonstrates the need for specialized codes. The problem has several complexities including phase change, rapid rotation, and vortices that Fluent must not be able to handle all at once. An algorithm designed specifically to accommodate rotating internal flow would be useful for this simulation. Ultimately, Fluent did provide a look at modeled buoyancy forces interacting with the body forces induced by rotation.

BIBLIOGRAPHY

"Air War College." Materials Volume – Fuels and Lubricants. 28 Nov. 2006<http://www.au.af.mil/au/awc/awcgate/vistas/match11.pdf>.

"Aviation Turbine Fuel Composition." Chevron Home Page. 2000. Chevron Products Company. June 4, 2007<http://www.chevron.com/products/>.

Bruno, Thomas J., Marcia L. Huber, Arno Laesecke, Eric W. Lemmon, and Richard A. Perkins. "Thermochemical and Thermophysical Properties of JP-10." October 2005.

Duangthip, Thammarat. "Simulations of Jet Fuel Thermal-Oxidative Degradation and Flow Characteristics of Injected Jet Fuel Under Supercritical Conditions." University of Dayton Dissertation, April 2004.

Edwards, Tim. "USAF Hydrocarbon Fuels Interests," Letter. Wright Patterson Air Force Base, Ohio.

Ervin, Jamie, Thomas A. Ward, Theodore F. Williams, and Jarrod Bento. "Surface Deposition Within Treated and Untreated Stainless Steel Tubes Resulting from Thermal-Oxidative and Pyrolytic Degradation of Jet Fuel." Energy and Fuels 17 (2003): 577 – 586.

Fluent Inc. Fluent 6.2 User's Guide. ANSYS Inc., Jan. 1, 2005.

Fox, Robert W., Alan T. McDonald, and Philip J. Pritchard. Introduction to Fluid Mechanics. 6th ed. John Wiley & Sons, Inc., 2004.

Huang, He, Louis J. Spadaccini, and David R. Sobel. "Fuel-Cooled Thermal Management for Advanced Aeroengines." Journal of Engineering for Gas Turbines and Power 126 (2004): 284 – 293.

Katta, V. R., J. Blust, T. F. Williams, and C. R. Martel. "Role of Buoyancy in Fuel-Thermal-Stability Studies." Journal of Thermophysics and Heat Transfer 9 (1995): 159 – 168.

Kuprowicz, Nicholas Jay. "A Predictive Modeling Approach to Simulate Liquid-Phase Oxidation and Deposition of Jet Fuels." University of Dayton Dissertation, April 2006.

Lemmon, Eric W., Mark O. McLinden, and Marcia L. Huber. "NIST Standard Reference Database 23 – NIST Reference Fluid Thermodynamic and Transport Properties – REFPROP." August 2002.

Maurice, L. Q., H. Lander, T. Edwards, and W. E. Harrison III. "Advanced aviation fuels: a look ahead via a historical perspective." Fuel 80 (2001): 747 – 756.

Morris, W. David. Heat Transfer and Fluid Flow in Rotating Coolant Channels. John Wiley & Sons, Inc., 1981.

Osmont, Antoine, Iskender Gokalp, and Laurent Catoire. "Evaluating Missile Fuels." Propellants, Explosives, Pyrotechnics 31, No. 5 (2006): 343 – 354.

Ramineni, Pradeep. "Simulations of Jet Fuel Flow with Imposed High Heat Flux." University of Dayton Graduate Thesis, August 2005.

Rao, P. Nageswara and Deepak Kunzru. "Thermal Cracking of JP-10: Kinetics and Product Distribution." Journal of Analytical and Applied Pyrolysis 76 (2006): 154 – 160.

"The National Academies Press." Evaluation of the National Aerospace Initiative Fuels Research. 2004<http://books.nap.edu/openbook.php?record_id=10980&page=122>.

Ward, Thomas A., Jamie S. Ervin, Richard C. Striebich, and Steven Zabarnick. "Simulations of Flowing Mildly-Cracked Normal Alkanes Incorporating Proportional Product Distributions." Journal of Propulsion and Power 20 (2004): 394 – 402.

Wilcox, David C. Basic Fluid Mechanics. 2nd ed. La Canada, Ca: DCW Industries, Inc., 2003.

Yu, J. and S. Eser. "Supercritical-phase Thermal Decomposition of Binary Mixtures of Jet Fuel Model Compounds." Fuel 79 (2000): 759 – 768.